CHALMERS
UNIVERSITY OF TECHNOLOGY

PHD THESIS

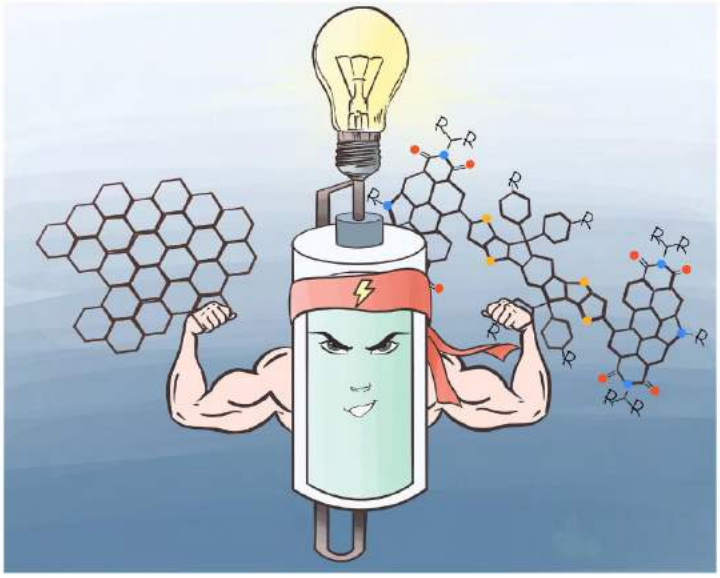

2D materials and conjugated small molecules: from synthesis to devices for energy applications

ULISES ANTONIO MÉNDEZ-ROMERO

DEPARTMENT OF CHEMISTRY AND CHEMICAL ENGINEERING
CHALMERS UNIVERSITY OF TECHNOLOGY
Gothenburg, Sweden 2021
www.chalmers.se

THESIS FOR THE DEGREE OF DOCTOR OF PHILOSOPHY

2D materials and conjugated small molecules: from synthesis to devices for energy applications

ULISES ANTONIO MÉNDEZ-ROMERO

Department of Chemistry and Chemical Engineering

CHALMERS UNIVERSITY OF TECHNOLOGY

Gothenburg, Sweden 2021

2D materials and conjugated small molecules: from synthesis to devices for energy applications
ULISES A. MÉNDEZ-ROMERO
ISBN 978-91-7905-597-4

Thesis for the Degree of Doctor of Philosophy
Serie Nr: 5064
in the series Doktorsavhandlingar vid Chalmers tekniska högskola.
Ny serie ISSN 0346-718X

Department of Chemistry and Chemical Engineering
Division of Applied Chemistry
Chalmers University of Technology
SE-412 96 Gothenburg
Sweden
Telephone + 46 (0)317721000

Cover:
[Artistic drawing by Mariza Mone illustrating a supercapacitor training with conjugated small molecule and graphene]

Chalmers Reproservice
Gothenburg, Sweden 2021.

2D materials and conjugated small molecules: from synthesis to devices for energy applications

Ulises Antonio Méndez Romero
Department of Chemistry and Chemical Engineering
Chalmers University of Technology

Abstract

The main goal of the present work is to contribute to the area of renewable energy storage, trough the precise engineering of 2D materials and conjugated materials. Thus, four different type of graphene-based materials and a conjugated small molecule were synthesized in order to successfully develop supercapacitors. In the case of the graphene-based materials it was possible to modify its main parameters such as lateral dimensions, dispersibility, and energy levels.

Furthermore, a new graphene-based material (SOG), that combines the advantages of GO and graphene without their disadvantages, was synthesized. SOG shows water dispersibility, a C/O ratio 260% higher than GO, and most importantly, a very high crystallinity degree, with an I_D/I_G of 0.414. The synthesized SOG exhibits an ultra-low optical band gap of 0.04 eV, which is 75 times lower compared to GO. Moreover, the electrical resistance is nine orders of magnitude smaller (1.12 KΩ/sq) compared to GO. In order to analyze the feasibility of SOG for energy storage application, a swagelok-based supercapacitor was fabricated which exhibited remarkable characteristics such as 16 474 mF g^{-1} of gravimetric capacitance, and good retention at 10 000 mV s^{-1} of scan rate. SOG characteristics make it a promising new material for applications in organic electronics.

Finally, a novel perylene diimide-based (PDI) and indacenodithieno[3,2-b]thiophene (IDTT) small molecule has been successfully synthesized and used for the first time as an organic-electrode supercapacitor. This new approach circumvents complex issues regarding the synthesis and purification of polymers. Promising results of a nanocomposite made of this SM and 10% SOG demonstrate a synergistic effect of 48.75% increase in the capacitance at 10 mA g^{-1}, in two-electrode cells for a practical demonstration in energy storage. This study may open new possibilities for fabricating supercapacitors and multifunctional devices from conjugated small molecules and graphene-based materials.

Keywords: *graphene-based materials, conjugated materials, energy storage, solution processing*

List of Publications

This thesis is based on the work contained in the following papers, referred to by Roman numerals in the text:

Paper I. Lateral size reduction of graphene oxide preserving its electronic properties and chemical functionality

U.A. Méndez-Romero, S.A. Pérez-García*, Q. Fan, E. Wang* and L. Licea-Jiménez*

RSC Advances **2020**, 10, 29432-29440. DOI:10.1039/D0RA04726K

Paper II. Functionalized reduced graphene oxide with tunable bandgap and good solubility in organic solvents

U.A. Méndez-Romero, S.A. Pérez-García*, X. Xu, E. Wang* and L. Licea-Jiménez*

Carbon **2019**, 146, 491-502. DOI:10.1016/j.carbon.2019.02.023.

Paper III. Long-term evolution of the chemical and structural stability of graphene oxide after storage as solid and as an aqueous dispersion

U.A. Méndez-Romero, M.A. Velasco-Soto*, L. Licea-Jiménez*, J. González-Hernández and S.A. Pérez-García*

Nano Select **2021**, 2, 2168. DOI:10.1002/nano.202000274

Paper IV. Selectively oxidized graphene with high crystallinity for applications in supercapacitors

A. Méndez-Reséndiz‡, U.A. Méndez-Romero‡, R.A. Mendóza-Jiménez, S.A. Pérez-García*, E. Wang* and L. Licea-Jiménez*

Submitted.

Paper V. A Perylene-diimide based Small Molecule as Binder-Free Electrode for High Energy Density Pseudocapacitors

U.A. Méndez-Romero‡, Birhan A. Abdulahi‡, Jingnan Wu, Qiaonan Chen, Guijun Yang Wendimagegn Mammo, Donghong Yu, S.A. Pérez-García*, L. Licea-Jiménez* and Ergang Wang*

Manuscript in preparation.

Paper VI. Nanocomposite based on Functionalized Graphene and Conjugated Small Molecule as Binder-free Solution-Processed Electrode for Supercapacitors

U.A. Méndez-Romero‡, Birhan A. Abdulahi,‡ Jingnan Wu, Qiaonan Chen, Guijun Yang Wendimagegn Mammo, Donghong Yu, and Ergang Wang*

Manuscript in preparation.

Contribution Report

Paper I. U.A.M.R. contributed to the conceptualization and conducted the major part of synthesis, methodology, characterizations, and writing.

Paper II. U.A.M.R. contributed to the conceptualization, and conducted the major part of synthesis, methodology, characterizations, and writing.

Paper III. U.A.M.R. contributed to the conceptualization, and conducted the major part of synthesis, methodology, characterizations, and writing.

Paper IV. Equal contribution from U.A.M.R. and A.M.R. U.A.M.R. contributed to the conceptualization, synthesis, methodology, characterizations, and writing.

Paper V. Equal contribution from U.A.M.R. and B.A.A. U.A.M.R. contributed to the conceptualization, methodology, characterizations, and writing.

Paper VI. Equal contribution from U.A.M.R and B.A.A. U.A.M.R. contributed to the conceptualization, methodology, characterizations, and writing.

Co-authored Publications Not Included in the Thesis

Paper A. Fluorinated Photovoltaic Materials for High-Performance Organic Solar Cells

Q. Fan, U.A. Méndez-Romero, X. Guo, E. Wang*, M. Zhang* and Y. Li

Chemistry – An Asian Journal **2019**, 14(18) 3085-3095. DOI:10.1002/asia.201900795

Paper B. Mechanically Robust All-Polymer Solar Cells from Narrow Band Gap Acceptors with Hetero-Bridging Atoms

Q. Fan, W. Su, S. Chen, W. Kim, X. Chen, B. Lee, T. Liu, U.A. Méndez-Romero, R. Ma, T. Yang, W. Zhuang, Y. Li, Y. Li, T.-S. Kim*, L. Hou*, C. Yang*, H. Yan, D. Yu, E. Wang*

Joule **2020**,4 (3), 658-672. DOI:10.1016/j.joule.2020.01.014

Paper C. Weak Makes It Powerful: The Role of Cognate Small Molecules as an Alloy Donor in 2D/1A Ternary Fullerene Solar Cells for Finely Tuned Hierarchical Morphology in Thick Active Layers

Q. Fan, T. Liu*, M. Zhang, W. Su, U.A. Méndez-Romero, T. Yang, X. Geng, L. Hou, D. Yu, F. Liu*, H. Yan*, E. Wang*

Small Methods **2020**, 4(3)1900766. DOI:10.1002/smtd.201900766

Paper D. Highly Stable Indacenodithieno[3,2-b]thiophene-Based Donor-Acceptor Copolymers for Hybrid Electrochromic and Energy Storing Applications

P. Murto‡, S. Elmas‡, U.A. Méndez-Romero, Y. Yin, M. Mone, G. Andersson, M.R. Andersson*, E. Wang*

Macromolecules **2020,** 53, 11106-11119 DOI:10.1021/acs.macromol.0c02212

Paper E. Improved charge storage performance of a layered $Mo_{1.33}C$ MXene/MoS_2/graphene nanocomposite

A. El Ghazaly, U.A. Méndez-Romero, J. Halim, E. Tseng, P. Persson, B. Ahmed, E. Wang and J. Rosén*

Nanoscale Advances, **2021** DOI: 10.1039/D1NA00642H

Paper F. Graphene-based scalable spin-coated heterogenous stacked electrodes for CMOS/MEMS compatible micro-supercapacitors for modular integration

A. Vyas*, S. Z. Hajibagher, U. A. Méndez-Romero, S. Thurakkal, Q. Li, M. Haque, E. Wang, R.K. Azega, X. Wang, P. Lundgren, P. Enoksson and A. D. Smith*

Manuscript submitted.

Paper G. Alkyl-amino Functionalized rGO-based Spin-coated Micro- supercapacitors for On-chip Low Power Electronics

A. Vyas*, S. Z. Hajibagher, U. A. Méndez-Romero, R. K. Azega, E. Wang, P. Lundgren, P. Enoksson and A. D. Smith

Manuscript submitted.

Book Chapter

Polymer coatings based on nanocomposites in Polymer Coatings: Technologies and Applications

L. Licéa-Jiménez, **U.A. Méndez-Romero**, A. Méndez-Reséndiz, A.R. Vázquez-Velázquez, R.A. Mendóza-Jiménez, D.F. Rodríguez-Díaz, S.A. Pérez-García

CRC Press, **2021**

Table of Contents

1. Introduction

The most critical issue that needs to be solved soon is energy production.[1] Fossil fuels have been widely used to meet the demands of mobility, product development, and mainly electric power production. Nevertheless, as this fuel is a finite resource and generates pollution, it is imperative to develop alternative technologies to satisfy energy demand.[2] One of the most explored technologies that eventually could overcome the energy problem is solar cells or photovoltaic cells (PVs). These devices convert electromagnetic radiation from the sun into electrical energy, which, in principle, could supply the energy needs with relative ease.[2]

The sun puts out 3.8×10^{23} kilowatt-hours of energy every hour. From that, 170 000 Tera Watts (TW) strike Earth every moment, nearly one-third of which are reflected into space, leaving "just" 120 000 TW. It means that every hour, Earth's surface receives more energy from the sun than humans use in a year. Covering 0.17 % of the Earth with 10 % power conversion efficient PVs would provide 20 TW of power, which is near twice the world's consumption rate of fossil energy.[3, 4]

Unfortunately, due to the intermittent renewable energy sources, other important aspects to consider are energy storage devices, such as supercapacitors, which have advantages compared to batteries: providing high power density (10 kW kg^{-1}), charge-discharge time in seconds and long-life cycle. In general, there are two types. One is the electrical double layer capacitor (EDLC), which stores energy via an electrostatic process, i.e., charges are accumulated at the electrode/electrolyte interface through polarization. The second type of supercapacitor is the pseudocapacitor, based on fast redox reactions of compounds in the electrode. The common electrode materials are metal oxides and conducting polymers. This type of electrode offers higher specific capacitance per unit surface area.[5]

In general, for supercapacitors, it is essential to use electrode materials with good conductivity and large specific surface areas such as graphene-based materials. The graphene-based materials, particularly rGO, are advantageous in terms of the chemically active surface with a

large specific area, good conductivity, low cost, and mass production with solution-based processability. [5, 6]

This thesis summarizes four papers focusing on the synthesis of graphene-based materials for energy storage applications. Pristine graphene is not suitable for direct use as an electrode for supercapacitors due to the lack of dispersibility and low-yielding synthesis (micromechanical exfoliation or CVD). To successfully use graphene, different approaches were developed. All the methods employed followed the top-down strategy to obtain materials in enough quantities (grams). The oxidation of graphite to produce graphene oxide (GO) make it water dispersible and originates an energy bandgap; however, the said bandgap is too wide (3 eV) to absorb visible light; however, a chemical remotion of oxygen (reduction) allows to control such bandgap. A common method is to do a chemical reduction; nevertheless, the resulting reduced graphene oxide (rGO) is not dispersible in water nor organic solvents. Another parameter to consider is the lateral size of the graphene-based material, which should be optimal to increase the specific surface area.

Thus, the applied strategy was to reduce the size of the GO after its synthesis. Still, it is important that such a process was done without modifying its properties (water dispersibility, band gap, C/O ratio, and functional groups). Afterwards, the smaller size GO is functionalized with octadecylamine (ODA) and chemically reduced (rGO-ODA).

However, the rGO-ODA has diminished crystallinity and requires organic solvents for processing. The general idea behind this type of device is to be the greenest possible; thus, the preferred solvents should be aqueous. Also, as stated previously, the criteria for a material to be used as an electrode for supercapacitors are good conductivity and redox activity. The GO is also a metastable material over time. In this context, it is clear that the GO and rGO are not good candidates for supercapacitors. Thus, the strategy developed was to synthesize a graphene-based material selectively oxidized (SOG). In this case, SOG has the advantage over GO, of being a water- dispersible material, but with low oxygen content as in rGO and the high conductivity like graphene. The final two papers discussed in this thesis are focused on an alternative to 2D materials, being a conjugated small molecule and its composite with functionalized SOG as electrode for applications in supercapacitors.

2. Aim and Scope

This work aims mainly to explore the production and properties of graphene-based materials as well as conjugated small molecules for energy storage applications. Even though huge research has been made in the field of 2D materials and conjugated small molecules, its synergetic combination remains challenging and must be further developed and studied. Several research questions regarding the synthesis and modification of graphene-based materials are still not answered and need to be addressed and clarified. The first question to be answered is:

Is it possible to synthesize graphene oxide and reduce its size to increase its specific surface area without compromising other parameters?

How stable is graphene oxide over time?

It is important to decrease the size of graphene-based materials to increase the specific surface area and form a more porous film for the application in energy storage. Also, for industrial applications, large amounts of materials and a relatively long storing period are required, isn't it reasonable to know how to keep the samples: dispersion or solid? And for how long should be the maximum storage time. In this regard, graphene oxide synthesized from modified Hummer's method is physically reduced in size by ultrasonic energy and analyzed over three years in water dispersion and as solid. However, since graphene oxide is insulating and dispersible in aqueous solvents, both because his C/O content, the following questions arise:

Is it possible to chemically reduce the graphene oxide and functionalize it to control its electronic and dispersibility properties?

How can we keep a good crystallinity of the graphene-based materials but make them dispersible?

It's possible to easily produce graphene oxide and modify it in terms of lateral size, dispersibility and electronic (C/O ratio), however, it is complex to recover the crystallinity of the starting graphite. In this regard, it is well known that a trade-off between dispersibility and electronic properties is contrary to the graphene-based materials' crystallinity. Therefore, a new approach to selectively oxidize graphene and keep all the benefits of graphene oxide and graphene without their drawbacks will be explored. Additionally, since the graphene-based

materials are sp^2 hybridized carbon atoms and other heteroatoms, analogously as conjugated small molecules hence, the final questions in this work are the following:

Can conjugated small molecules be used as the only component for electrode in supercapacitors?

Is it possible to combine graphene-based materials with the conjugated small molecule to improve the performance of supercapacitors?

The general considerations of the materials design and synthesis in this work are presented in Chapter 3. The different supercapacitor parameters are described in Chapter 4. Chapter 5 is based on the papers I to IV and describes how to synthesize and modify the graphene-based materials to optimize their further application. Finally, Chapters 6 and 7 are based on the papers V and VI, respectively, and describe the application of the conjugated small molecule, and the nanocomposite formed by this small molecule and a graphene-based material.

3. 2D materials based on graphene

3.1 Graphene

Graphene is a single layer of carbon atoms bonded in a hexagonal array (honeycomb-like, see Figure 1) with sp^2 hybridization (see 2.3) that exhibits a vast number of outstanding characteristics, making it one of the most promising two-dimensional (2D) materials. In general, the properties of 2D materials arise from the quantum confinement effects along the z-axis, leading to unusual electronic and surface characteristics. For instance, graphene possesses high optical transmittance (>97% from 400 to 1000 nm), thermal conductivity (~5000 W m^{-1} K^{-1}), high Young's modulus (~1.0 TPa), large specific surface area (2630 m^2 g^{-1}), and extraordinary carrier mobility (2.5 x 10^5 cm^2 V^{-1} s^{-1}), attributed besides of quantum confinement to the interaction of electrons with the periodic potential of graphene's honeycomb lattice. In this way, the crystalline structure and the said sp^2 domain gives rise to relativistic massless Dirac fermion behavior of electrons that obey Dirac's equation instead of the Schrödinger's equation.[7-9]

Moreover, graphene is a zero-band gap material due to its π-band (bonding π molecular orbital) and π^*-band (antibonding π^* molecular orbital) having a characteristic shape of Dirac cones, touching at the Dirac points.[8] Hence, most attention is focused on graphene applications for transparent and flexible electrodes.[10] Nevertheless, certain applications, as specific bandgap (E_g), highest occupied molecular orbital (HOMO) and lowest unoccupied molecular orbital (LUMO) energy levels, good dispersibility in organic solvents as well as a low cost that graphene can achieve when is subjected to certain chemical modifications, in other words, a graphene-based material.[11]

3.2 Graphene-based materials

Based on the properties mentioned above, there is a variety of research on graphene-based materials applied in green energy such as fuel cells, solar cells, lithium-ion batteries, supercapacitors, dye-sensitized solar cells, and photo-electrochemical cells for hydrogen evolution via water splitting.[12] In particular, previous work related to the use of graphene

derivatives in OPVs mainly focuses on graphene as the hole transporting layer, the electron transporting layer, and the active layers, showing satisfactory results.[13-16]

Graphene oxide (GO) is the most studied graphene-based material, which essentially is graphene with oxygen functional groups: hydroxyl, carboxyl, epoxy, and carbonyl. GO exhibits a wide optical band gap (E_g^{opt}) of 3 eV and, therefore, HOMO and LUMO levels.[11] The poor dispersibility in organic solvents, mismatching energy levels, large E_g as well as high electrical resistance ($\sim 10^{11}$ Ω)[17] due to the loss of crystallinity in GO limit its applications in organic electronics.

Since sp^2 domains and E_g in GO are related to C/O ratio, a promising strategy will be to reduce the amount of oxygen by chemical reduction reactions, which leads to another graphene-based material: reduced graphene oxide (rGO) with a narrower E_g and, therefore, higher conductivity ($\sim 7.5 \times 10^4$ S m^{-1}).[18] These chemical reactions can be carried out with harmful compounds like $NaBH_4$, N_2H_4, etc., or innocuous fructose in aqueous dispersions. However, both methods have the inconvenience of restacking the layers, which results in poor dispersibility.[19]

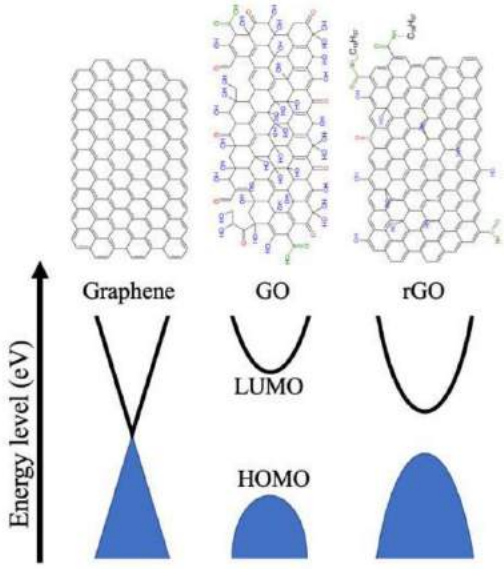

Figure 1 Structure of GO, rGO, and graphene, as well as their energy levels.[20]

3.3 Conjugated small molecules

In a molecule with at least two adjacent sp^2 hybridized carbon atoms, the sp^2 hybrid orbitals form single (σ) bonds. In contrast, the non-hybrid *p*-orbitals form a double (π) bond between the carbon atoms, as shown for ethene in Figure 2a). In a larger structure, such as buta-1,3-diene (Figure 2b)), the π-bond electrons can diffuse (*i.e.,* delocalize) along the neighboring *p*-orbitals, known as conjugated system. The conjugated *p*-orbitals together form new molecular orbitals, which share the electron density depending on the phase of each *p*-orbital. In the case of buta-1,3-diene, a total of four molecular π-orbitals are formed, as illustrated in Figure 2c). The π-electrons occupy the two lower-energy (in-phase, bonding) molecular orbitals, leaving the two higher-energy (out-of-phase, antibonding) molecular orbitals unoccupied. The energy difference between the HOMO and LUMO is called bandgap. Interestingly, the shared π-electrons between the *p*-orbitals reduce rotational torsion between the carbon atoms, which planarizes the conjugated structure.[21, 22]

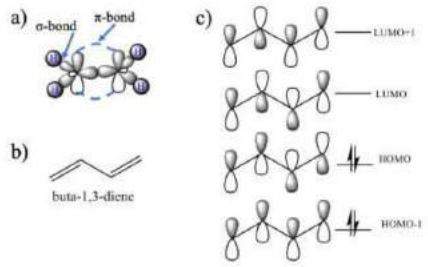

Figure 2 a) σ- and π-bonds in ethene molecule; b) Chemical structure of buta-1,3-diene and c) illustration of the conjugated *p*-orbitals.[22]

The ultimate advantage of conjugated materials is their tunable properties such as bandgap, molecular energy levels, carrier mobility, morphology, among others. A general strategy to synthesize a conjugated small molecule (SM) is by combining an electron-rich monomer (donor) and electron-deficient monomer (acceptor) in order to polymerize a D–A alternating conjugated SM. When the donor unit is bonded to the acceptor unit, it results in a D-A conjugated small molecule that has a linear combination of molecular orbitals, *i.e.*, the HOMO of the SM is similar to the HOMO of the donor monomer, while the LUMO of the SM is similar to the LUMO of the acceptor monomer, resulting into a lower bandgap and therefore capable of accepting more electrons, as seen in Figure 3.[22]

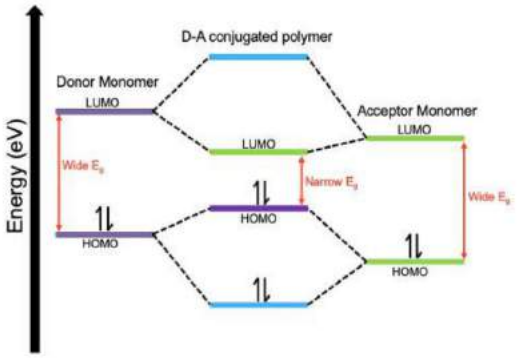

Figure 3 Linear combination of frontier molecular orbitals.[22]

Recently a D-A set of polymers based on indacenodithieno[3,2-*b*]thiophene (IDTT) were synthesized with the specific aim of introducing electrochemically stable alternatives to the 3,4-ethylenedioxythiophene-based polymers.[23] This was confirmed since those polymers showed excellent long-term switching stabilities, manifested by preserving 80–98% of their initial optical contrast after 1800 charge-discharge cycles and maximum capacitance of 260 F g^{-1} in a three-electrode set-up.[23]

On the other hand, a very attractive acceptor unit is based on perylenediimide (PDI). PDI-based compounds are a relevant type of active optoelectronic materials with application in several fields: organic photovoltaics (OPVs)[24, 25], organic field-effect transistors[26], sensors[27, 28], etc. It is essential to mention that PDI is a relatively inexpensive and common industrial pigment material. They have a tuneable band gap, strong π-π interactions, low energy levels, high stability (thermal, chemical, and photochemical), strong electron-acceptor character comparable to fullerene derivatives, high electron mobility. Moreover, the simple functionalization at the aromatic core and imide positions allows good tuning of their solubility and energy levels.[29-31]

There are few publications regarding energy storage studies centered on PDI-based polymers.[32-35] In those four previous publications, the results are excellent. Nevertheless, the addition of rGO[34] or carbon black[32] made a synergistic effect. A flexible SCs fabricated with D-A polymer based on PDI and benzodithiophene (BDT) blending with 16.6 wt. % carbon nanotubes show an areal capacitance of 350 F m^{-2} and almost 100% retention over 4000

cycles.[35] It is important to point out that polymers have drawbacks such as difficulties for purification and batch-to-batch variations on molecular weight. Conjugated small molecules, on the other hand, have extra advantages of easy purification, well-defined structures, and good reproducibility in synthesis. However, such a promising class of materials has not been explored as an electrode for supercapacitors.

4. Supercapacitors

Another application is related to the energy storage devices like supercapacitors (SCs). Compared to batteries, SCs exhibit higher power density but lower energy density. SCs are one application where 2D materials can significantly increase performance and efficiency. SCs are unique because they provide a much higher power density than conventional batteries while having a higher energy density than regular capacitors maintaining almost limitless cycling durability. Depending on the working mechanism, SCs can be divided into three main categories: Electrical double-layer capacitors (EDLCs) that primarily work on physical separation of charge forming electrical double layers (EDLs) near the surface of the electrode. Their performance is dependent on the surface area of the electrode, pore size, and electrical conductivity; Pseudocapacitors use fast reversible redox reactions at the electrode-electrolyte interface, resulting in Faradaic charge transfer. Because the latter have much higher specific capacitance due to redox reactions, they often suffer from performance degradation from repeated charge-discharge cycles.[36, 37] Hybrid devices that combine both capacitors- and battery-like processes in energy storage. Based on the device configuration, SCs can also be classified as symmetric or asymmetric devices.

The stored energy (E) in a capacitor is proportional to the capacitance (C) and voltage (V), where the maximum operating voltage depends on the stability of the electrolytes. In contrast, the capacitance relies on the active material from the electrodes.[36, 37]

$$E = \frac{1}{2}CV^2$$

Equation 1. Stored energy in a capacitor.

The specific capacitance (C_{sp}) of the thin film electrodes capacitors can be calculated from the CV plots using Equation 2.[36, 37]

$$C_{sp} = \frac{\int I(V)dV}{vA\Delta V}$$

Equation 2. Stored energy in a capacitor from CV.

Where $\int I(V)dV$ is the integral of the CV plot, v is the scan rate (V/s), A is the electrode area (cm^2), and ΔV is the potential range of the CV scan.[36, 37]

However, another way to obtain the capacitance is by the information obtained from galvanostatic charge-discharge (GCD) plots allow to use a simple equation to calculate the specific capacitance, Equation 3 and plot it against the current applied[38]:

$$C_s = \frac{I \cdot \Delta t}{\Delta V \cdot m}$$

Equation 3. Stored energy in a capacitor from GCD.

Where I is current, Δt is discharge time, ΔV is the potential window, and m is the total loading mass of the device.

4.1 Electrical Double-layer Supercapacitors

The Electrical Double-Layer (EDL) is described by the Helmholtz mechanism as the reversible electrostatic accumulation of two ion-sized layers of opposite charges on the interface between an electrolyte and the surface of an electrode that is polarized (Figure 4a). Decades later, Gouy and Chapman adjusted Helmholtz's model by keeping in mind the ion diffusion. Here the potential decreases exponentially from the interface to the rest of the electrolyte solution, as seen in Figure 4 b). Later, Stern combined both models to consider two regions of contribution: The stern layer and the diffuse layer (Figure 4c). Then capacitance of the EDL (C_{EDL}) is then defined by the sum of the capacitance of Stern layer (C_H) and diffuse layer (C_D) that corresponds to a connection in series:

$$\frac{1}{C_{EDL}} = \frac{1}{C_H} + \frac{1}{C_D}$$

Equation 4. Capacitance from EDLCs

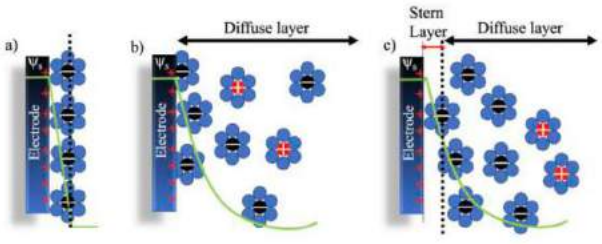

Figure 4 Double layer models: A) Helmholtz, B) Gouy and Chapman, and C) Stern

4.2 Pseudocapacitors

Capacitance originated by fast reversible redox reactions and not by an electrostatic mechanism is called *pseudocapacitance*. For instance, in pseudocapacitors, active materials on the electrodes' surface experience electrochemical charge transfer while applying a potential difference, like batteries; yet the working principle is different. Essentially, batteries keep a relatively constant voltage until they are fully charged or discharged as it follows the Nernst equation. Meanwhile, the capacitance from EDLS and pseudocapacitors is not continuous at changing voltages. Thus, its derivate defines pseudocapacitance:

$$dC = \frac{dq}{dV}$$

MnO_2 is one of the most studied materials used to fabricate pseudocapacitors, with suitable theoretical capacitance, conductivity, and availability in nature. Nevertheless, in practice, the bulk material shows low performance; thus, it limits loading MnO_2 on the surface of the electrode. Other metal oxides like RuO_2 show significantly higher performance, but despite the improvement compared to other materials, RuO_2 is more expensive. Therefore, its scalability for mass production is unlikely. Conjugated polymers exhibit pseudocapacitive mechanisms that offer high conductivity and are more lightweight and portable. The downside for polymers is the lack of thermal stability and their processing conditions.[38]

4.3 Hybrid Supercapacitors

Usually, the low specific power density from pseudocapacitive materials needs to be overcome by combinations with carbon-based materials; hybrid supercapacitors are a new alternative that uses different energy storage mechanisms: redox reactions and EDLCs. In other words, a synergy of materials boosts the specific energy density by using the high specific surface area and conductivity of carbon materials and the high capacitance from redox-active materials.

Hybrid supercapacitors are classified depending on their configuration: asymmetric, composite, and battery-capacitor. Asymmetric hybrids use one EDLS electrode and a pseudocapacitive electrode; it has been shown that by doing this, an improvement of capacitance, compared to normal EDLS and better cycle-life than pseudocapacitors is

obtained. Indeed, the battery-capacitor configuration has an asymmetric form, but the high-capacity principle corresponds to a battery. Moreover, they use the advantages of EDLS and batteries that show desirable opportunities to fill the gap between them to reach fast charging-discharging devices with high specific energy and long cycle-life. Naturally, by using two different energy storage mechanisms, compatibility issues arise; therefore, more optimization of the conditions of the materials is required, in addition to finding the right combination.

In hybrid composites, the materials are integrated more effectively. The high specific surface area from the EDLCs material improves the contact with the pseudocapacitive materials and allows a more uniform electrode that works more synergistically with its components.

5. Synthesis and modification of graphene-based materials for supercapacitors

This chapter gives a general overview of the synthesis methods and materials characterization before device fabrication and characterization. The graphene-based materials are usually characterized by X-ray photoelectron spectroscopy (XPS) and Raman spectroscopy, but also by Attenuated total reflection Fourier transform infrared (ATR-FTIR) where possible. The HOMO and LUMO energy levels of the polymers are measured by cyclic voltammetry (CV). Optical properties are examined by UV-Vis-NIR absorption. An electronic microscope was used to analyze the morphology. A set of standard CV, Galvanostatic charge-discharge (GCD), cyclic charge-discharge (CCD), and electrochemical impedance spectroscopy (EIS) were performed to characterize the devices.

5.1 Graphene Oxide. *Paper I, II, III*

The synthesis of graphene oxide starts from graphite nanoparticles (GNPs), using the modified Hummers' method reported previously.[11] Briefly, 0.5 g of GNPs were oxidized in 30 mL of H_2SO_4 and 0.295 g of KNO_3 with 3 g of $KMnO_4$ to achieve the formation of Mn_2O_7 complex. The reaction was carried out for 6 hours, stirring the solution at 450 rpm controlling the temperature below 15 ºC. The reaction was quenched with 100 mL of DI H_2O and 6 mL of H_2O_2 30%, see Figure 5 a). Next, the obtained bright yellow dispersion (graphite oxide) was centrifuged at 3500 rpm for 10 minutes to remove the supernatant, and 100 mL of HCl 10% were added to the precipitate and centrifuged under the same conditions. The washing process was repeated three times with DI H_2O. Afterward, 80 mL of DI H2O were added, and the dispersion was placed in the ultrasonic bath for 1 hour for exfoliation, see Figure 5 b). Finally, the supernatant in water dispersion was recovered, stored, and labeled as GO.

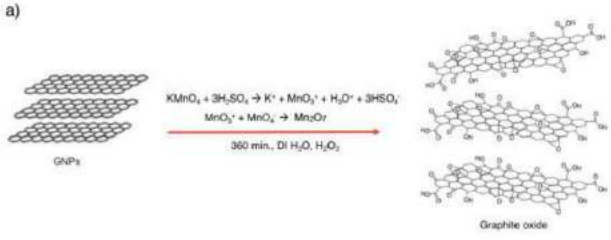

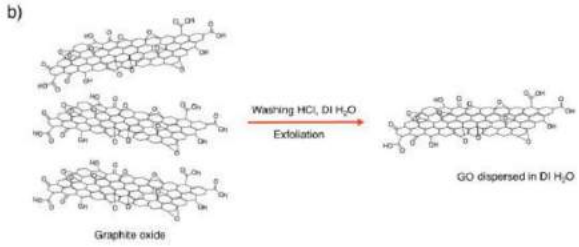

Figure 5 a) Schematic representation of the synthesis of graphite oxide. b) Schematic representation of the synthesis of graphene oxide

5.1.1 Morphology modification. *Paper I*

The obtained GO aqueous dispersion resulted in an E_g^{opt} of 3 eV. The lateral size decrease of GO was achieved by a Branson sonifier model SFX250, applying a 40% amplitude and a controlled temperature of 18°C. The procedure was performed as follows: the starting GO dispersion (GO-0) was diluted at [3 mg mL^{-1}] and gauged to 10 mL followed by sonication.

Every 30 minutes for a lapse of 240 minutes, 1 mL of the GO dispersion was taken and gauged at 10 mL in centrifuge vials named GO-30, GO-60, GO-90, GO-120, and GO-240, referring to the time in the ultrasonic probe. Later, the dispersions were centrifuged at 3500 rpm for 1 hour to remove the less stable GO. Then the supernatant was analyzed. See a schematic representation in Figure 6.

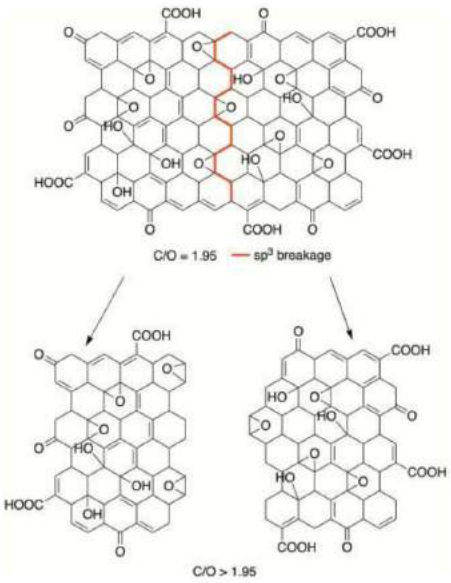

Figure 6 Schematic representation of the size reduction mechanism in the x-y plane, without modification of the C/O ratio.

5.1.2 Stability. *Paper II*

GO could be considered a precursor for graphene-like structures through its chemical, thermal, or photoreduction. It could be highly desirable to be stored for an indefinite time for later studies or use.

In this context, there are scarce reports that address the issue of GO chemical self-reduction over time, that is, its metastability. Kim et al. studied the change of oxygen concentration in GO films over one hundred days under light and oxygen at ambient conditions. In short, the analysis reveals that solid GO should be kept under dark conditions. Also, Chua et al. stored GO powder for 30 weeks to study an approach to restrain its chemical modification in different conditions. It was found that darkness and inert atmosphere conditions preferred methods to maintain GO with a high O/C ratio. To preserve a high O/C ratio is important to achieve good dispersion of GO in water or other polar solvents and maintain the chemical groups for further functionalization.

As previously mentioned, most related works on GO storage were done in samples stored in solid form. GO is produced through aqueous processes, such Hummers method, and commonly dried for further use. GO is easier to handle as liquid dispersion, saving time and energy to re-disperse the solid GO.

For this analysis, two aliquots of GO were adjusted to 6 mg mL^{-1}, then transferred into two beakers followed by dry filtering at 25°C for 48 hours with the aid of Whatman 0.2µm PTFE vacuum membranes. At the top of the membrane, a reddish-orange GO solid could be peeled off. Samples were stored in sealed petri dishes for two periods: one year (sample labeled as GO-1S) and three years (sample labeled as GO-3S). The storage conditions were at room temperature, darkness, and ambient pressure.

In order to study the effect of liquid storage, GO aqueous dispersion was adjusted to 6 mg mL^{-1} and stored in two different vials in darkness, ambient temperature, and ambient pressure as standard conditions. GO liquid samples were stored and analyzed after one year (labeled as GO-1L) and three years (labeled as GO-3L).

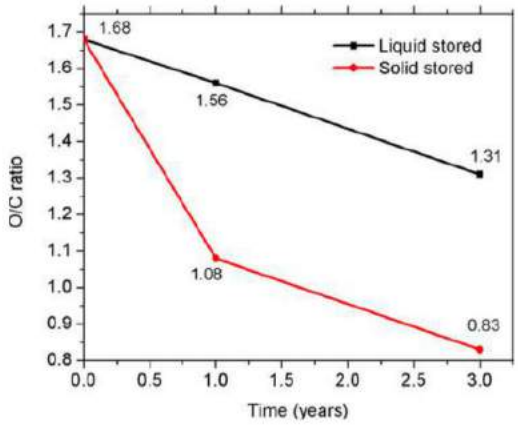

Figure 7 The plot of the O/C ratio for liquid stored GO and solid stored GO was obtained from high-resolution XPS C1s.

For GO, GO-1L, GO-3L, GO-1S, and GO-3S, values of $R_{O/C}$ were obtained and displayed in Figure 7, where it results evident that the significant decrease in O/C ratio corresponds to the

solid samples. The O/C retention, in the case of solid stored, has a dramatic drop of its values being 64% and 49% for GO-1S and GO-3S, respectively, while for liquid stored, GO-1L slightly drops the O/C ratio retention from 93% to 78% for GO-3L.

5.1.3 Solubility and Electronic Modification

Starting from the GO, a phase transfer from water to a desired organic solvent was performed to achieve an electrostatically functionalized GO with octadecylamine (GO-ODA). The functionalization of the fresh synthesized GO dispersed in water, fixed at [10 mg mL^{-1}] to *o*DCB or toluene was performed electrostatically by mixing a solution of ODA in ethanol [30 mg mL^{-1}] in a 1:1 volume ratio and sonicated for 5 minutes.[11]

The mixture was stirred at 450 rpm for 5 minutes at room temperature. Subsequently, an equal volume of the desired solvent (*o*DCB or toluene) was added and stirred at 450 rpm for 3 minutes at room temperature, promoting a phase transfer. The organic phase (GO-ODA) was stored for later use. In Figure 8, it is shown a schematic diagram representing this process.

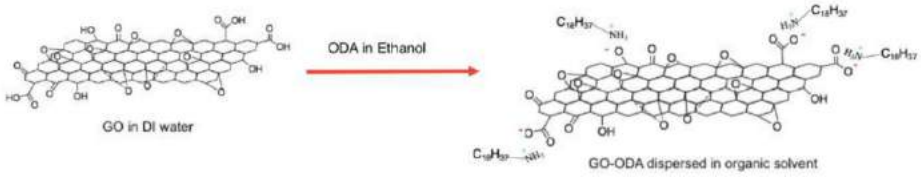

Figure 8 Electrostatic functionalization by ODA.

Finally, the chemical reduction reaction was carried out by adding 100 µL of ascorbic acid-6-palmitate (AA6P) [100 mM] solution in *o*DCB or toluene for each 100 mg of GO, at 98 °C and stirred at 450 rpm for 2 hours. Thus, reduced graphene oxide functionalized with ODA (rGO-ODA) was obtained in solution. The sample was vacuum filtered in a Pall PTFE membrane with a diameter of 47 mm and 0.2 µm pores and dried at room temperature for further characterization

The proposed mechanism of the chemical reduction reaction is described below in Figure 9. In summary, the ascorbic acid-6-palmitate reduces the epoxy groups, while the carboxyl and carbonyl are thermally reduced. Because carboxyl is electrostatically bonded to the amine, the reaction allows a condensation, creating a covalent bonding with water as a by-product, which eventually evaporates from the reaction media. [11]

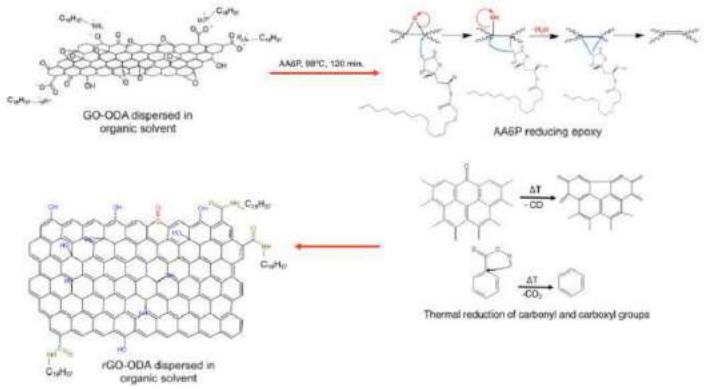

Figure 9 Proposed mechanism for the chemical reduction. [11]

5.2 Selectively Oxidized Graphene. *Paper IV*

First, 30 mL of a solution of concentrated H_2SO_4 and 0.295 g of KNO_3 were added to 0.5 g of GNPs. Then 0.3 g of $KMnO_4$ was slowly added to the mixture while using a water bath at 14 °C. This amount of $KMnO_4$ is a tenth from the standard ratio 6:1 ($KMnO_4$: graphite)[11]. Subsequently, the reaction was allowed for 30 minutes in the water bath, which means that the reaction time was decreased twelve times, compared with our previous work (6 hrs.)[11]. Afterward, the mixture was centrifugated at 4500 rpm for 10 min. Then the supernatant was discarded, and the precipitate was washed with 10% HCl followed by another centrifuge washing steps (3 times) with DI water.

The obtained precipitate was dispersed in DI water using an ultrasonic bath for one hour. Figure 10 shows a schematic representation of the whole process.

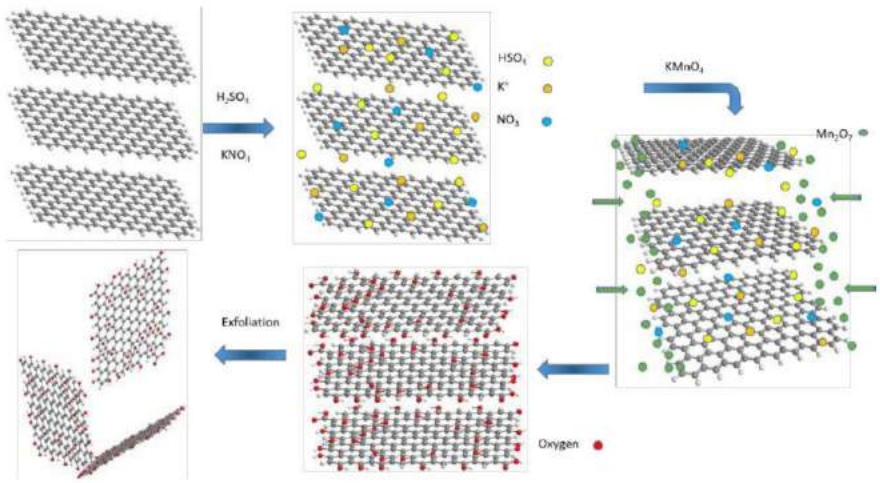

Figure 10 Proposed selectively oxidation mechanism of SOG.

5.3 XPS of Graphene-Based Materials

The XPS is an extraordinary technique to analyze graphene-based materials (GBMs) since it provides an insight into the different atoms bonded to the carbon. The GBMs used in this thesis presented three representative signals in the high-resolution C1s spectra recorded from 279 eV to 298 eV.: C-C, C-O, and C=O at 284.48 eV, 286.88 eV, and 288.88 eV, respectively. [11, 19]

To easily understand the changes during the different chemical modifications, the starting graphitic material is also included. The C1s core level spectra are shown in Figure 11, where Figure 11 a) corresponds to GNPs and Figure 11 b) to GO. The signal coming from the GNPs is composed only by C-C, with a single contribution at 284.48 eV. The absence of any other signal reveals purity and crystallinity of the material, proving at the same time information that no previous oxidation is present. After Hummer's method, the obtained GO shows completely different spectra, agreeing with a highly oxidized material. [11, 19]

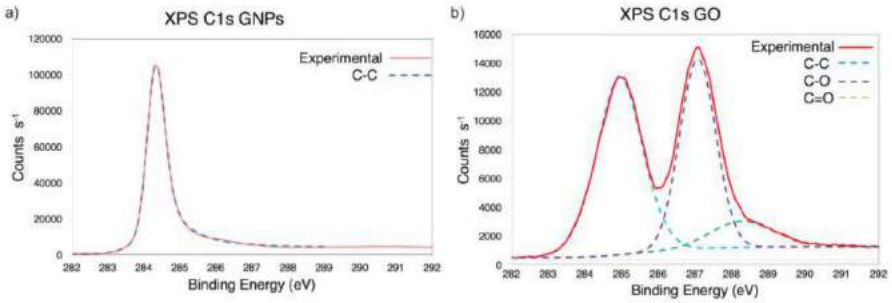

Figure 11 High-resolution XPS C1s analysis of a) GNPs and b) GO

The subsequent modification done was a lateral size reduction. It was previously stated that the materials intended to be used as active layers should have a smaller size than the thickness of the layer itself [39]. Interestingly, the lateral size decreases without compromising other relevant parameters, such as C/O ratio, crystallinity, and bandgap. It was described in the methodology section that the process involved sonification through time of GO. Thus, GO-0 corresponds to a GO without treatment, GO-30 corresponds to a material that was kept for 30 minutes in the ultrasonic probe, and so on. The lateral size reduction for the GOs showed a slight difference (less than 3%) in the C/O ratio, as seen in Figure 12.

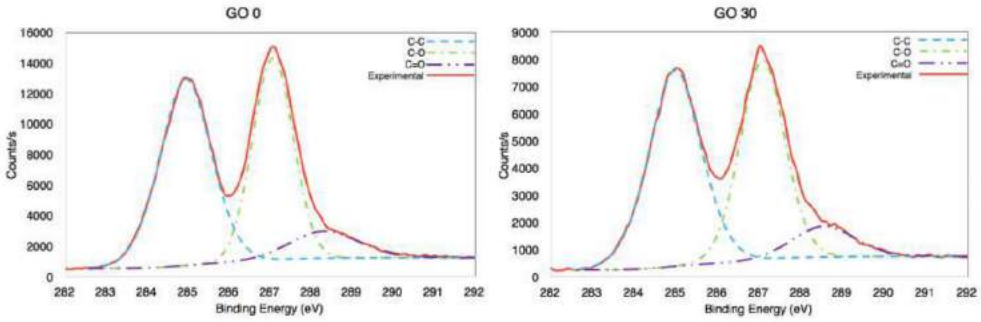

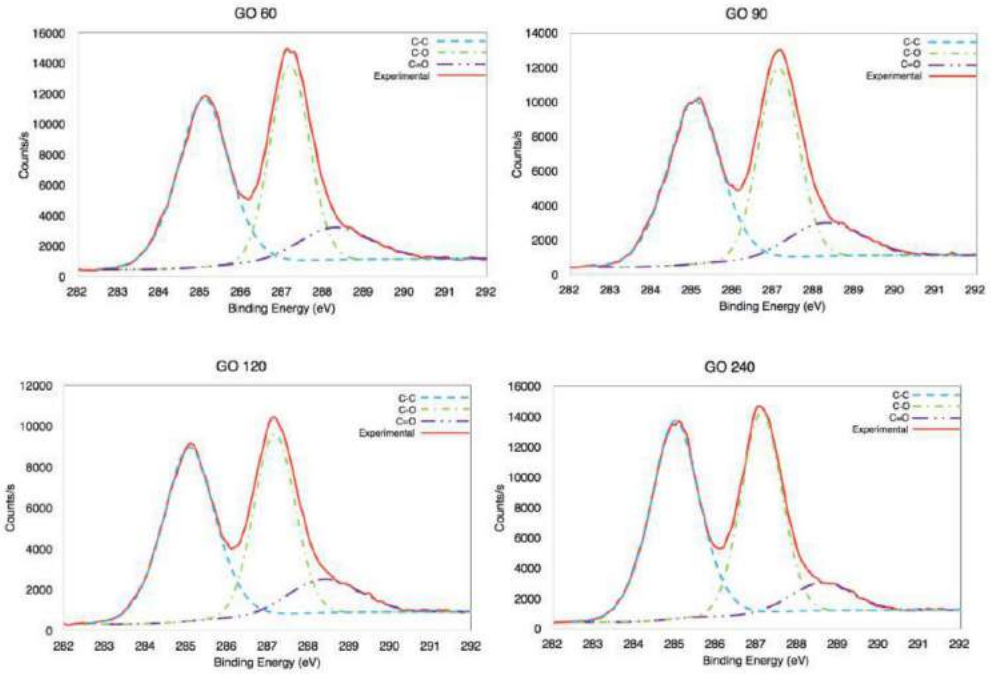

Figure 12 High-resolution XPS C1s analysis of GOs after 0, 30, 60, 90, 120, and 240 minutes of sonication.

To analyze the relation between lateral size against the applied energy during sonication, the plot in Figure 13 shows the progression in size reduction depending on the energy during the experiment. The significant change in size is achieved during the first stage of the experiment (first two hours). However, based on the plot, one can interpolate or extrapolate the required energy to obtain a specific desired size. This plateau behavior could be explained by the depletion of sp^3 breakage areas, confirming that the mechanism is related to the lowest bond dissociation energy (BDE) by mechanical vibration [40].

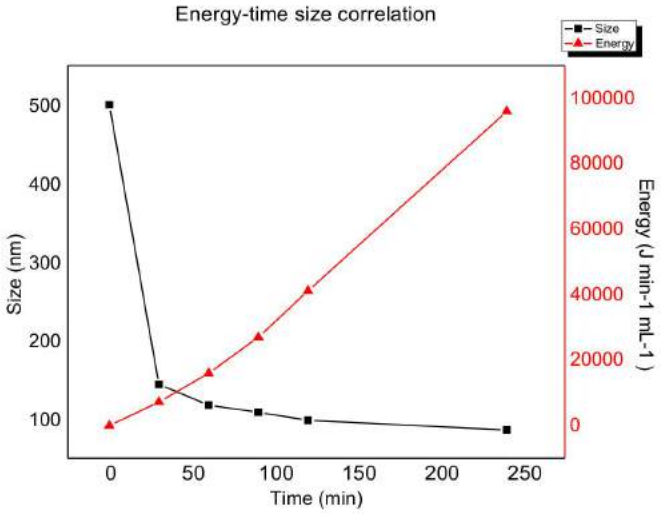

Figure 13 Lateral size obtained by Dynamic Light Scattering vs time and applied energy during sonication.

As can be noticed, the XPS results were divided into three groups, Figures 11, 12, and 14. The first group are the starting material and the intermediate (GO), the second group, Figure 11 shows the modification of the intermediate and the third group of materials, in Figure 14 it is shown the high-resolution C1s from GEX, SOG, and rGO-ODA, which are the final products, that were applied in the fabrication of devices. As one can see, the spectra obtained from GEX is very similar to the starting GNPs, with just a tiny amount of carbonyl (<1%). Deconvoluted peaks of the SOG in Figure 14 b) show oxygen functional groups due to the oxidation reaction. It is clear that even when the oxidation occurs under mild conditions and just 30 minutes, it is enough to introduce oxygen functionalities into the structure. The signal coming from rGO-ODA in Figure 14 c) is characteristic of a highly reduced state, presenting a minimal contribution of C-O at 288.08 eV and a new signal related to C-N at 285.48 eV, suggesting a covalent functionalization by ODA.[11]

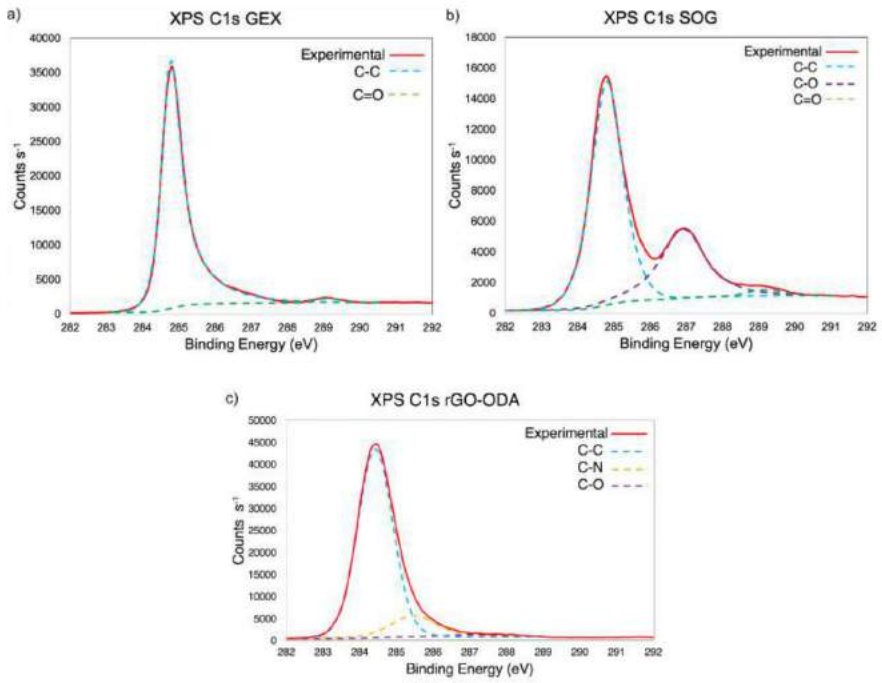

Figure 14 High-resolution XPS C1s analysis. a) GEX, b) SOG, and c) rGO-ODA.

In Table 1, the C/O ratio from all the GBMs is presented. One of the main advantages of this type of materials, is the capability to tailor the oxygen content and therefore its properties: optical band gap, HOMO-LUMO energy levels, dispersibility and further functionalization. The GBMs are incredibly diverse, and in Table 1, it is clear that they were successfully modulated in the most critical parameter, besides the size.

Table 1. C/O ratio for the Graphene-Based Materials

Material	C/O ratio	Dispersibility
GNPs	∞	None
GO	1.95	H_2O
GEX	199	H_2O:CH_3OH
SOG	3.48	H_2O
rGO-ODA	99.77	$CHCl_3$

It is essential to mention that these values are exciting. Of course, the results from the GNPs and GO are expected and previously reported. [41, 42] However, a previous report from our research group found a C/O ratio of 3.25 for its highest reduced GO [19], which is even more oxidized than the synthesized SOG, proving the advantage of this new material. Because this new material does not require a reduction process to achieve the said oxidation degree and, more importantly, keeping a good dispersibility in water, conversely to the reported rGO [19]. The rGO-ODA is a highly reduced material, even when compared with an rGO annealed at 1000ºC [41]. In the case of the GEX, the C/O ratio is comparable to the graphene obtained by chemical vapor deposition (CVD)[43], which is remarkable.

5.4 Raman Graphene-Based Materials

To compare the structural quality of the graphene-based materials, Raman spectra (Figure 15) recorded with 2.33 eV laser energy are presented. It is well known that the particular dispersion of π electrons in graphene offers powerful and efficient insights into their electronic properties, and therefore of their crystallinity. It can be noticed that all spectra exhibit an intense band from 1450-1660 cm^{-1} corresponding to the *G* band due to vibrational E_{2g} degenerative mode observed in sp^2 carbons. Furthermore, another band is observed at 1260-1400 cm^{-1}, assigned to the *D* band and related to the A_{1g} mode. The *D* peak is originated due to the interaction between phonons and defects, such as in-plane substitution heteroatoms, vacancies, or grain boundaries.[44-46]

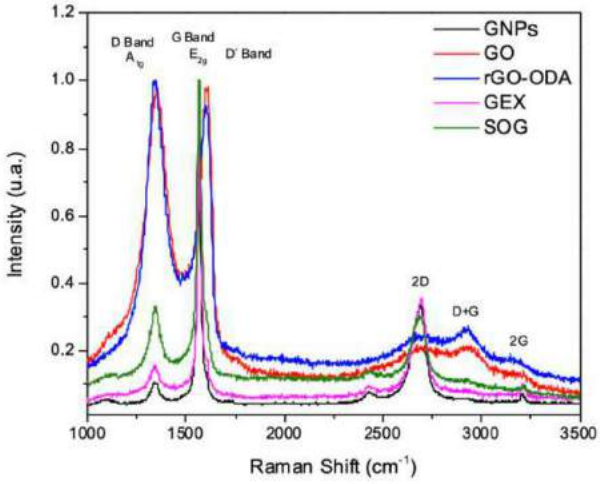

Figure 15 Raman Graphene-Based Materials

For better clarity, the section between 1200 to 1700 cm^{-1} is presented in Figure 16. In this regard, previous studies [47, 48] used *D* peak to quantify the number of defects in graphene through the intensity (peak integrated area) ratio of *D* and *G* peaks (I_D/I_G).

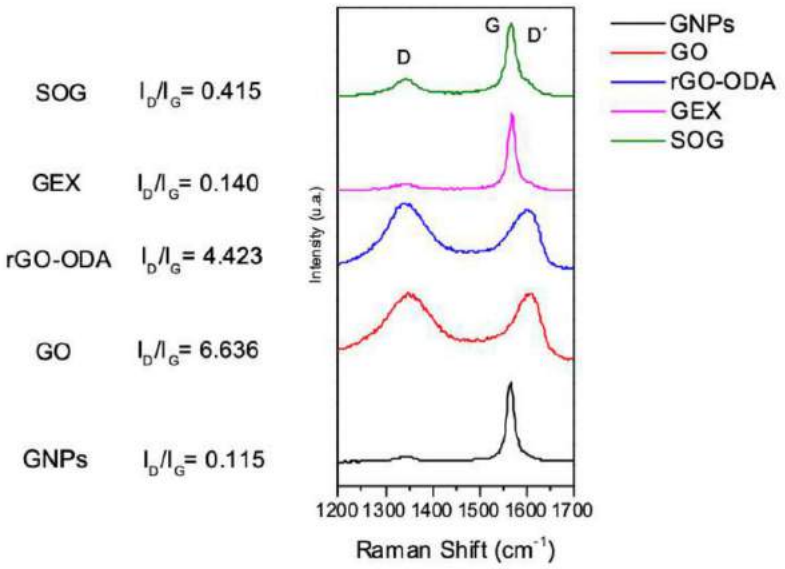

Figure 16 The crystallinity of Graphene-Based Materials by Raman.

As expected, the material with the best crystallinity is the starting GNPs, since they were not subjected to any process. The GO has the lowest crystallinity, but interestingly, the rGO-ODA does not recover the crystallinity, despite the highly chemical reduction shown in the XPS results. It is worth pointing out that the I_D/I_G value for SOG is almost 16 times lower than GO and 47 times lower when compared to the GEX. These results indicate that GEX and SOG exhibit crystallinity that is more related to graphene grown by CVD [43, 49, 50] rather than GO or rGO, which is excellent considering the simplicity of the method and its scalability.

5.5 Electron microscopy

This section allows us to assess the morphology of the synthesized 2D materials from the raw material and after the synthesis process. In Figure 17, the scanning electron microscopy (SEM) micrograph from the starting graphite nanoparticles (GNPs) is presented. As can be noticed, it consists of a graphitic material composed of several layers stacked together. The lateral size of this starting material is around 500 to 800 nm.

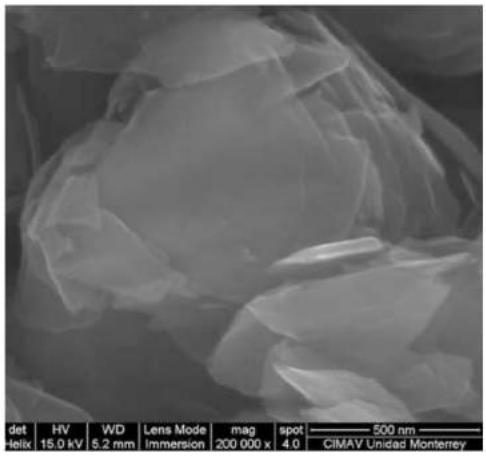

Figure 17 SEM micrograph from the starting GNPs

In the case of the precursor GO, as previously established, it was subjected to a lateral size reduction. In Figure 18, the micrographs from scanning transmission electron microscopy (STEM) are presented. Figure 18 a) shows the starting GO without any modification, and Figure 18 b) shows the GO after the ultrasonic treatment. It is clear that a lateral size reduction was achieved. In both cases, a single-layer material is displayed, as can be seen by the contrast difference in the micrography, with the characteristic wrinkles.

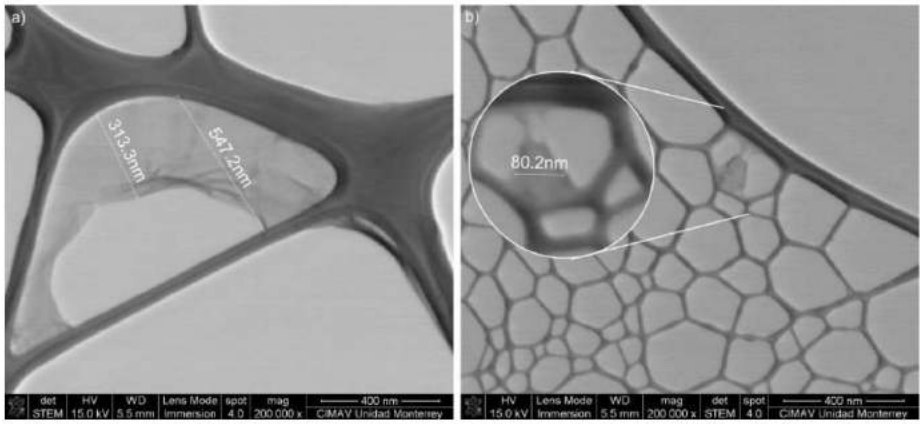

Figure 18 STEM from the GO, a) starting GO and b) GO after size-reduction

The rGO-ODA and SOG are presented in Figure 19 a) and b), respectively. In both cases, they appear flattered when compared to the GO. But in a single layer material. The lateral size is similar in both materials.

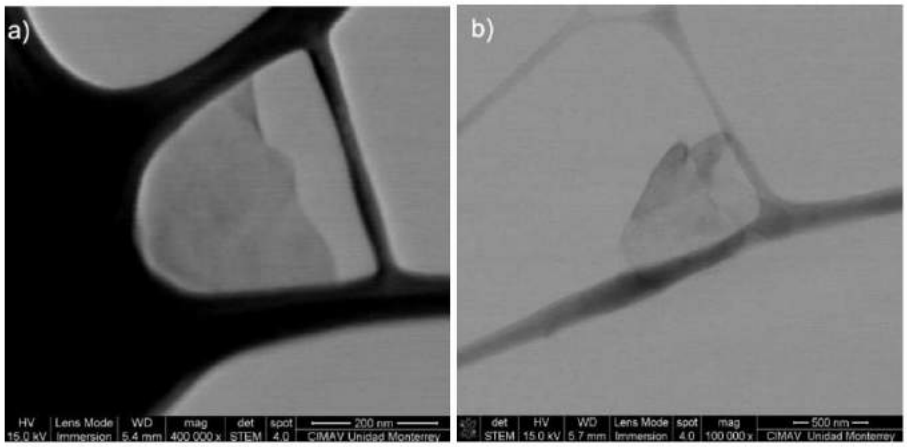

Figure 19 a) STEM micrograph from rGO-ODA. b) STEM micrograph from SOG

5.6 Viability of energy storage: Supercapacitors

The capacitive energy storage capability was analyzed by comparing SOG against pristine exfoliated graphene, both from the same starting GNPs. SOG and exfoliated graphene were assessed in a Swagelok configuration supercapacitor in order to compare the superiority of SOG over exfoliated graphene in the same conditions. The cyclic voltammetry (CV) curves were collected and are presented in Figure 20. It can be seen that both devices exhibit almost rectangular CV curves as an indicator of a nearly ideal capacitive behavior [51], which is maintained even at highly high scanning rates (up to 50,000 mVs^{-1}).

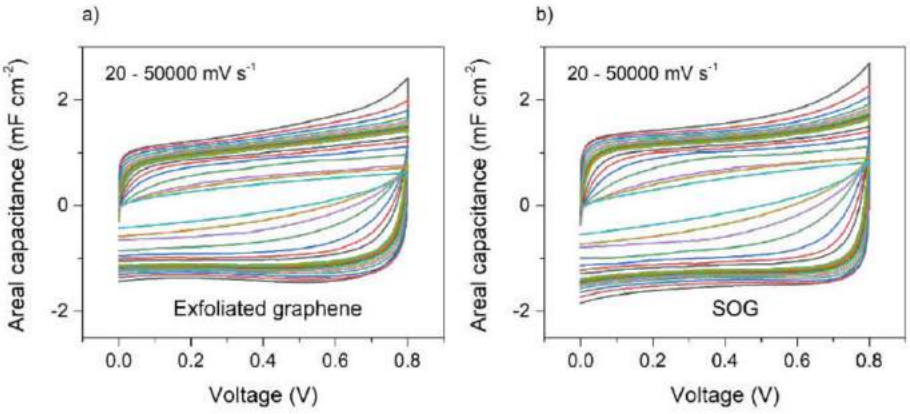

Figure 20 Symmetric supercapacitor performance from cyclic voltammetry curves at different scanning rates from 20 mV s^{-1} up to 50 000 mV s^{-1} of a) exfoliated graphene and b) SOG in 1.0 M $NaSO_4$.

The specific capacitance for both devices was obtained from the electrochemical measurements and is presented in Figure 21. It can be seen in Figure 21 a) that the SOG values of gravimetric capacitance are greatly enhanced from 1275 mF g^{-1} to 16474 mF g^{-1} from exfoliated graphene to SOG, respectively; this behavior could be attributed to a better-exfoliated material and the enhanced redox activity provided from the oxygen groups. In Figure 21b), an improvement of ~17% in the areal capacitance is achieved for SOG with the highest value of 7.12 mF cm^{-2} and 65% retention (4.62 mF cm^{-2}) at a scan rate of 1000 mV s^{-1}. These results are higher than values reported for equivalent supercapacitors based only on exfoliated graphene [52]. From these results, it is clear the great advantage of using SOG instead

of exfoliated graphene. One should remember that GO is a dielectric material and is not suitable for this application in its pure state. In this context, it is evident that SOG takes advantage of graphene and GO without their limitations.

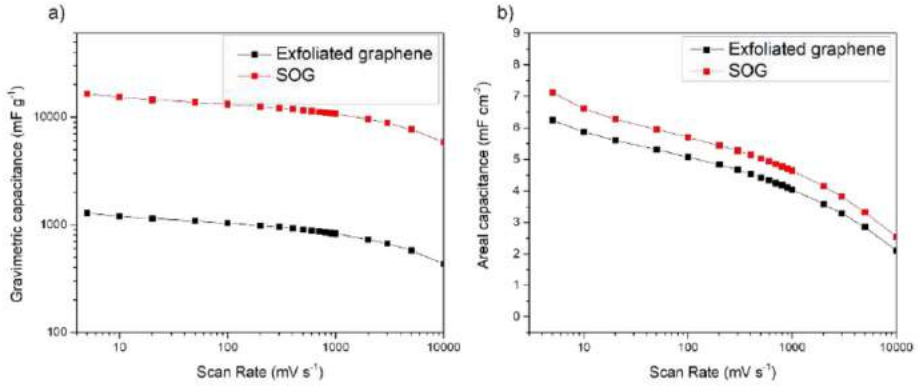

Figure 21 Comparison of the capacitance values obtained from the electrochemical measurements for exfoliated graphene and SOG is shown as a) gravimetric capacitance and b) areal capacitance at different scan rates.

A nearly perfect triangular shape can be observed when looking at the galvanostatic charge-discharge (GCD) curves in Figure 22 a-b). The almost linear behavior demonstrates that the predominant nature of the charge storage is due to the electric double-layer capacitance[53]. Also, the charge-discharge time is increased in the SOG device to indicate the enhanced charge retention.

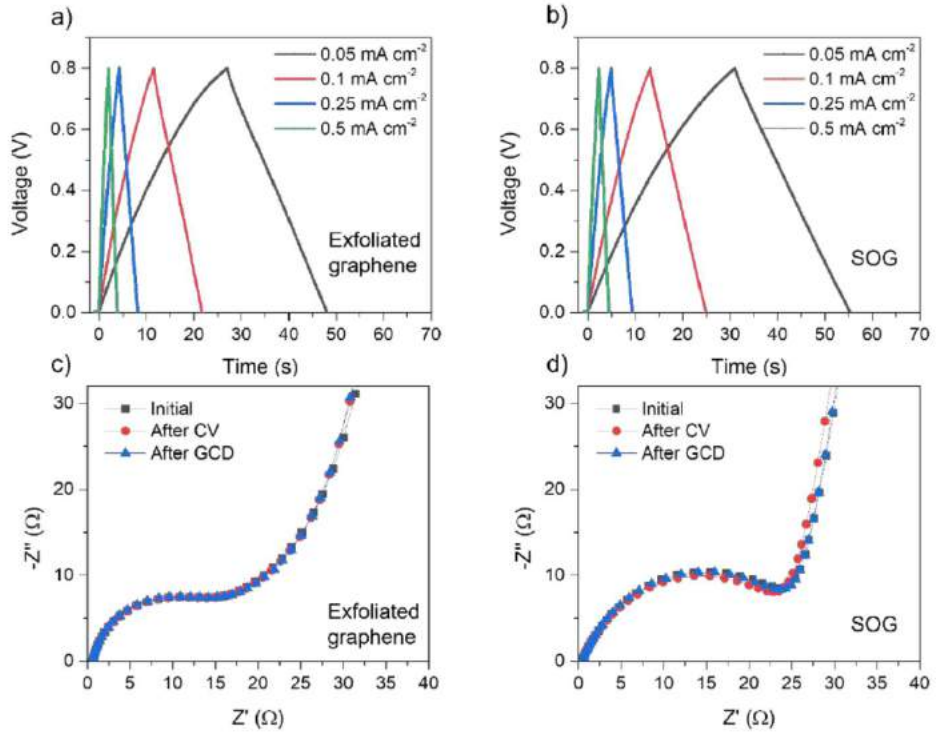

Figure 22 Electrochemical characterizations of the devices. Galvanostatic charge-discharge of a) exfoliated graphene and b) SOG. Electrochemical Impedance Spectroscopy was used to analyze Nyquist plots for c) exfoliated graphene and d) SOG.

Based on the Electrochemical Impedance Spectroscopy (EIS) analysis (Figure 22 c-d), the internal resistance (R_s) is obtained from the intersection with the *x*-axis at high-frequency [51], resulting in values of 0.684 and 0.55 Ω for exfoliated graphene and SOG, respectively. Also, the width of the semicircle represents the charge transfer resistance (R_{ct}) which is higher for SOG due to the introduction of oxygen functionalities. Nevertheless, its high stability is remarkable since the Nyquist plots in Figure 22 d) do not show variations after the measurements.

6. Characterization of Conjugated Small Molecules based Supercapacitors

6.1 Design and synthesis of an SM for supercapacitors. Paper V

As schematically illustrated in Figure 23, PDI-IDTT-PDI SM was synthesized by standard Stille coupling reaction between the brominated PDI and the stannylated IDTT core. The molecule was purified using column chromatography and recrystallization over acetone. The detailed synthesis procedure of the PDI-IDTT-PDI SM can be found in the electronic supporting information of Paper V. This molecule was designed considering not only the donor and acceptor nature of IDTT and PDI, but also the incorporation of the alkyl sidechains in PDI provides an excellent solubility in organic solvents for solution processability. Moreover, the amide functionalities of the PDI units are essential to enhance the redox activity of the SM.

Density functional theory (DFT) calculations at the B3LYP/6-31G (d, p) level were done to assess the 3D conformational structure of the PDI-IDTT-PDI SM. To simplify the calculation, the alkyl side chains were replaced by methyl groups. The calculated dihedral angle between the IDTT core and the PDI end groups is 63.55°. Despite both PDI and IDTT being large planar units, the large torsion dihedral angles, as indicated by the DFT calculation, helps to prevent the tight π-π stacking and improve ion diffusion due to the exposed surface increasing free volume. Therefore, the resulting film is expected to facilitate ion mobility. All this was considered to differentiate from conventional planar systems where strong π-π stacking reduces solubility and impedes ion motion.

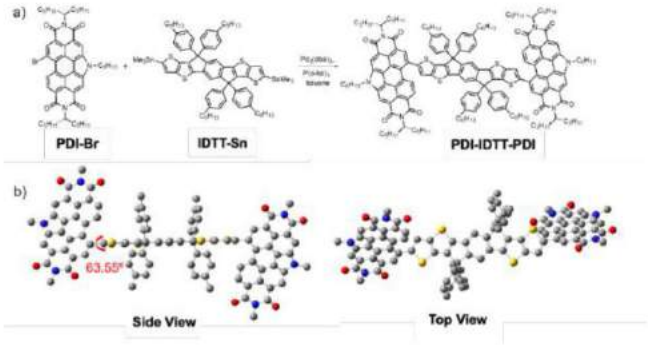

Figure 23 a) Synthesis of the PDI-IDTT-PDI SM by Stille-coupling reaction. b) Side and top views of the optimized geometry of PDI-IDTT-PDI SM by DFT.

The LUMO energy levels associated with the PDI moieties are more energetically accessible than those associated with the IDTT moieties (Figure 24), being -3.21 eV and -1.51 eV, respectively from DFT calculations. Figure 24b illustrates the charge-storage mechanism of PDI-IDTT-PDI SM: the PDI moiety accepts two electrons[32], for a total of 4 electrons per SM as seen in Figure 24 a).

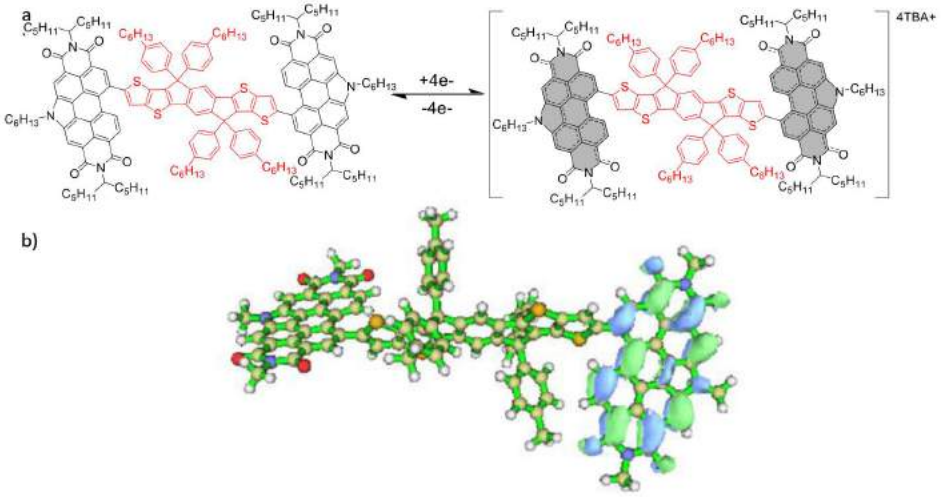

Figure 24 a) Proposed mechanism for charge storage within the PDI-IDTT-PDI SM. b) Lowest unoccupied molecular orbital (LUMO) level of the PDI-IDTT-PDI SM. Different colors MOs indicate opposing phases.

6.2 PDI-IDTT-PDI Conjugated Small Molecule for supercapacitors

To evaluate the performance of the SM in SCs, a standard Swagelok cell was employed. The PDI-IDTT-PDI SM was dissolved at a concentration of 4 mg mL^{-1} in dichloromethane, and 150 µL were dropped cast directly on the metal collectors, 0.6 mg of the active material per electrode. Subsequently, one collector was placed in a Swagelok cell and 100 µL of gel electrolyte (Poly(methyl methacrylate) 40% wt. dissolved at 50ºC for 4 hours in 1M solution of tetrabutylammonium hexafluorophosphate in anhydrous acetonitrile) was added to cover the entire surface. A glass microfiber separator was then placed, and the other collector was finally placed in the cell, and the device was assembled. To assess the capacitance of the PDI-IDTT-PDI SM, a three-electrode set-up was performed, with a platinum wire as working and a counter-electrode, using Ag/Ag^{+} as the reference electrode and the same gel electrolyte

previously described. The specific capacitance from CV at one mV s^{-1} was 343 F g^{-1}, and the total energy stored in the system was 1543 J g^{-1} due to the large potential window of 3V, which is among the highest value for PDI-based polymers.

Subsequently, a sequence of electrochemical measurements were done in a symmetrical two-electrode system: 1. Electrochemical Impedance Spectroscopy (EIS) initial; 2. Cyclic Voltammetry (CV) at increasing scan rates (SR) (3 cycles at every SR): 2, 5, 10, 20, 50, 100, 200, 300, 400, 500, 600, 700, 800, 900 and 1000 mV s^{-1}; 3. EIS after CV; 4. Galvanostatic Charge-Discharge (GCD) at increasing current densities: 0.05, 0.1, 0.25, 0.5, 0.75, 1, 1.25, 1.5, 1.75, 2, 2.5, 2.75 and 3 mA cm^{-2}, 5. EIS after GCD; 6. Cyclic Charge-Discharge (CCD) for 8000 cycles at 0.1 mA cm-2; 7. EIS after CCD.

The information obtained from GCDs allows us to explore its capacitance property further. As shown in Paper V, experiments of PDI-IDTT-PDI films shows that the capacitance is ion-diffusion controlled and belongs to a typical pseudocapacitive behavior since there is not a linear relationship between the scan rates and the current densities of the redox peaks.[54]

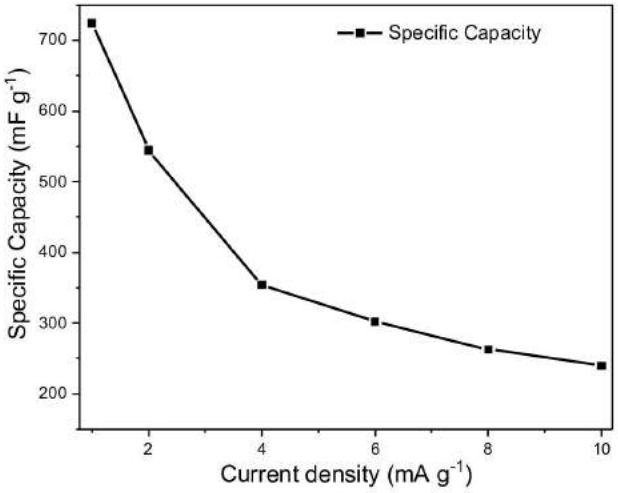

Figure 25 Capacitance retention over increased scan rates.

It was worth noticing that a capacitance shown in Figure 25 of 724 mF g^{-1} at 1 mA g^{-1} was recorded in Swagelok cell, which is indeed promising, especially considering that this is the very first SM-based device in a symmetrical device structure, the mass loading of PDI-IDTT-

PDI is as low as 1.2 mg without binder or conductive agent. Moreover, the SM can be processed from solution in organic solvents.

Next, to assess the capacitance retention over the CGCD at a constant current density of 1 A g^{-1}, it was performed for 10,000 cycles. As shown in Figure 26, the capacitance retention (C/C_0) can maintain over 85% after 10,000 CGCD, demonstrating outstanding stability of the PDI-IDTT-PDI SM-based SC devices. As seen qualitatively in the Nyquist plots at different stages as an inset in Figure 26, after all the CVs, GCDs, and CGCD, the device shows an evolution in the charge transfer in the electrode/electrolyte interface, implying a lower ion diffusion towards the electrode surface. This could be attributed to the acetonitrile evaporation in the gel electrolyte after several electrochemical measurements.

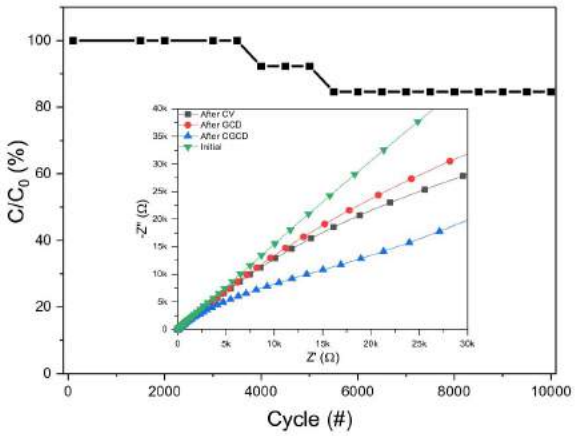

Figure 26 Capacitance retention over 8000 Cycling Charge-Discharge. The inset shows the evolution of the Nyquist plot over the electrochemical sequence.

To further verify the SM's chemical stability and understand CCD results, a chemical structure assessment was done utilizing Attenuated Total Reflection Fourier Transformed Infrared spectroscopy (ATR-FTIR). Figure 27 shows the ATR-FTIR spectrum from the pristine compound PDI-IDTT-PDI as a black line, a "fresh" device just made with the only purpose to be assembled and opened without any electrochemical test (red line). The SM recovered from the device after the 8000 CCD (blue line). It is essential to mention that both samples, from the fresh and the used device, had some gel electrolyte. Nevertheless, the results are identical from both samples in all the spectral regions, making evident that no chemical change

occurred, at least indicated by ATR-FTIR. However, as seen by Nyquist and CCD, something is happening since the capacitance is decreased by 15% after the charge-discharge cycles.

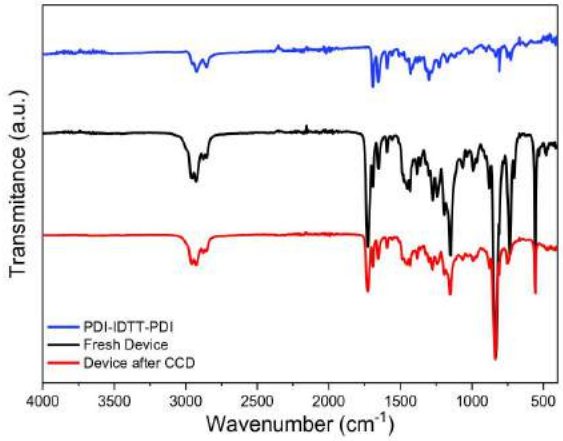

Figure 27 ATR-FTIR spectra of the pristine SM and the SM recovered from the device after CCD. The inset shows CVs of the initial device and after CCD.

7. 2D Materials and Small Molecule Composite for Supercapacitors

A common strategy for using graphene-based materials in Supercapacitors (SCs) is to incorporate them in a polymer matrix. Commonly, redox polymers are used due to their capability of electron exchange/transfer. Most used conjugated polymers with clearly defined isolated redox functionalities are poly (3,4 ethylene dioxythiophene): poly (styrene sulfonate) (PEDOT–PSS), polypyrrole, and polyaniline. The application of these materials as an anode is challenging. Also, the organic materials' capacities are comparatively low (mostly < 100 mAh g^{-1}). Hence electrodes with conjugated polymer-based nanocomposite have been developed.[55] In this regard, several studies have been carried out by incorporating graphene-based materials into the polymeric matrix, having promising results in terms of energy storage such as 584.7mF cm^{-2},[56] 2.98 μWh cm^{-2},[57] 18.9 mF cm^{-2},[58] 16.3 Wh kg^{-1},[59] 1300W kg^{-1},[60]. The other drawbacks of supercapacitors' current state of the art are related to the electrolytes that are typically strong acid or strong bases. The use of electrodes such as lithium or gold is scarce and expensive.[56-61] Therefore, it is essential to use eco-friendly electrolyte and metal-free electrode materials for practical applications.

Nevertheless, an inherent problem of the polymers relies on its difficulties for purification and batch-to-batch variations on their molecular weight. Conjugated small molecules, on the other hand, have extra advantages of easy purification, well-defined structures, and excellent reproducibility in synthesis. However, such a promising class of materials has not been explored as an electrode for SCs. Herein, we report, for the first time, a two-electrode Swagelok cell SC device made from a nanocomposite electrode of a conjugated small molecule (SM) based on PDI and IDTT and a heptadecane-9-amine functionalized selectively oxidized graphene (SOG-op). These well-defined molecular units (PDI and IDTT) are selected due to their unique structures and robust electrochemical properties on top of their appreciable twisting molecular conformation to avoid unfavorable aggregation. It is demonstrated in this work that the SOG-op PDI-IDTT-PDI nanocomposite electrode has excellent electrochemical properties, particularly high capacitance, fast charge-discharge, and higher than 86% capacitance retention after 10,000 charge-discharge cycles, due to its good chemical stability. Moreover, the addition of highly crystalline and dispersible graphene-based material allows

the solution processability of the devices without binders, thus forming a good electrode film with the potential of high capacitance. A functional symmetric supercapacitor comprising the composite of SOG-op and PDI-IDTT-PDI electrodes were fabricated and utilized as an energy storage device, featuring the potential of the small molecule systems for supercapacitor development.

The morphology was determined by transmission electron microscopy (TEM). Figure 28 shows the TEM micrograph for the SOG-op, where the material presents an individual flake structure. The lateral dimensions are around 2 microns. Furthermore, it is worth mentioning that SOG-op does not exhibit any crumpling, a common feature in GO, and reduced GO[62-65]; instead, a completely flat morphology is presented, indicating that the material is only slightly oxidized, maintaining almost its original structure and, therefore, avoiding the unnecessary introduction of defects. Based on these results, it is suggested that the synthesized material exhibit an outstanding combination of crystallinity, conjugated network preservation, and remarkable dispersion stability (with a zeta potential of -36 mV).

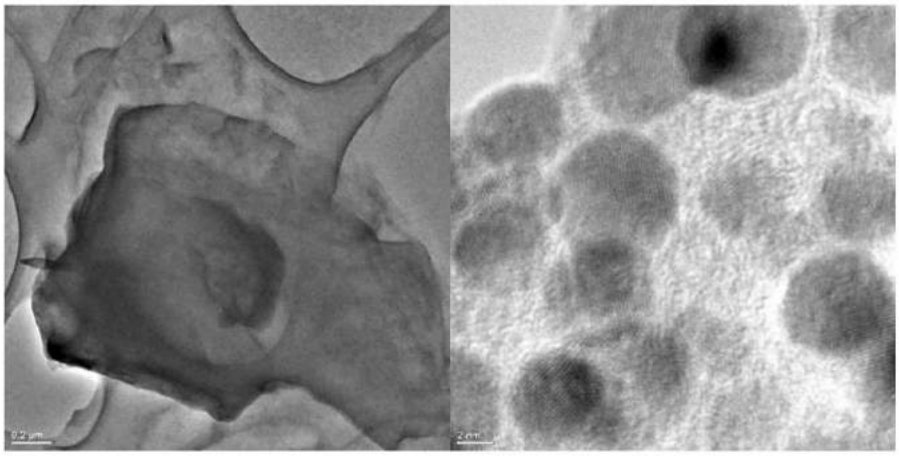

Figure 28 TEM micrographs of the Functionalized Graphene.

A standard symmetric Swagelok cell was employed to evaluate the practical performance of the nanocomposite of SOG-op-SM in SCs. A sequence of electrochemical measurements was done in a symmetrical two-electrode Swagelok cell: 1.) Initial electrochemical impedance spectroscopy (EIS) from 100 kHz to 0.01 Hz at AC voltage of 5 mV rms and 0 V DC; 2.) CV at increasing scan rates from 5 to 1000 mV s^{-1} from 0 to 2V, showing an excellent rate

capability preserved over the scan rates. 3.) EIS after the CV; 4.) Galvanostatic Charge-Discharge (GCD) at increasing current densities of 1, 2, 4, 6, 8, and 10 mA g^{-1} at 1 and 2 V 5.) EIS after the GCD; 6.) Cyclic Galvanostatic Charge-Discharge (CGCD) for 10,000 cycles at 0.1 A g^{-1}; 7.) EIS after the CGCD.

To understand the charge-storage kinetics of the nanocomposite and demonstrate its capacitive behavior, CV at different scan rates were performed between 5 to 1000 mV s^{-1} as shown in Figure 29 a) and b). Figure 29 c) displays a log-log plot of the scan rate (v) versus the peak current (i). These parameters obey the power-law given in Equation 6[66]:

$$i \propto v^b$$

Equation 6. b-Value relationship

The b-value can be obtained from the slope of the linear fit of the log i vs. log v plot is b (see Figure 29 c)). The slope of the plot indicates the charge storage mechanism. The b-value of 0.5 indicates a diffusion-controlled Randles–Ševčik behavior, whereas the b-value of 1 corresponds to a purely surface-controlled charge-storage process. Herein, the b-value at 2V from the lowest rate up to 1000 mV s^{-1}, as obtained from the slope of the linear fit is 0.64, indicating a combination of diffusion- and surface-controlled processes.

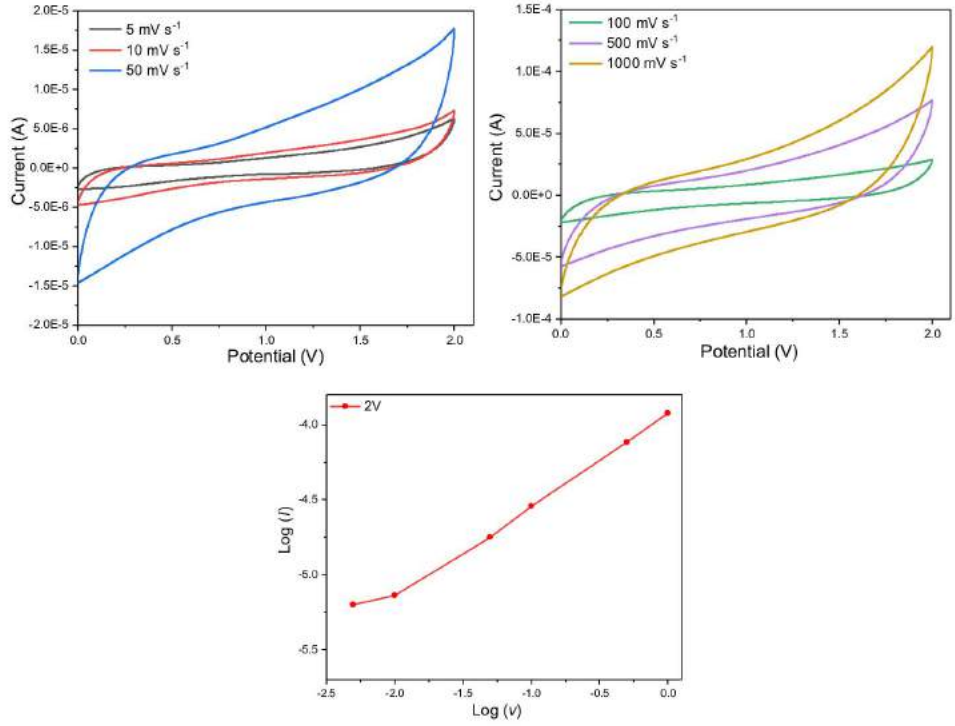

Figure 29 a) and b) CV curves of the SOG-op PDI-IDTT-PDI nanocomposite at different scan rates from 5 to 1000 mV s^{-1}. c) log *i* vs. log *v* plot at 2V

To assess the capacitance of the device, different current densities are presented in Figure 30. As one of the most crucial electrochemical characterization, GCD results show asymmetrical shapes with a slight curvature due to the redox reactions[67] in the amide functional groups in the PDI units and the carbonyl groups in the SOG-op, therefore, a pseudocapacitive behavior. It is also appreciated in Figure 30 that the capacitor is ion-diffusion controlled with typical pseudocapacitive behavior since there is no linear relationship pronounced between specific capacitance and current densities:[54, 68, 69] at a low current density, the discharge time is several times longer than that at higher ones.

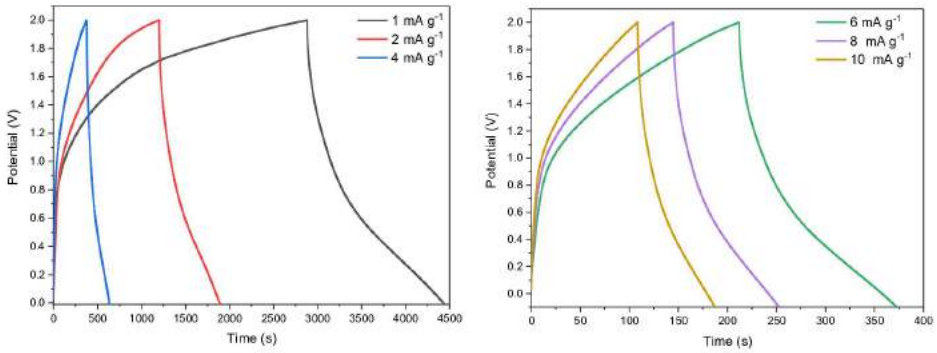

Figure 30 Galvanostatic charge-discharge at different current densities from 1 to 10 mA g^{-1}.

The information obtained from GCDs allows to use of a simple equation to calculate the specific capacitance (see Equation 3) and plot it versus the current density applied[38]. Accordingly, the specific capacitance at different current densities is summarized in Figure 31.

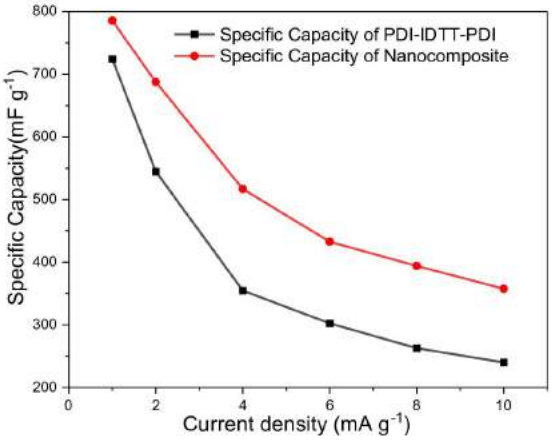

Figure 31 Capacitance retention over increased current densities.

It was worth noticing in Figure 31 that a capacitance shown of 785.89 mF g^{-1} at 1 mA g^{-1} was recorded in Swagelok cell, which is indeed promising, especially considering that this is the very first SM-based nanocomposite with 10% SOG-op content device with a symmetrical structure, the mass loading of the composite is as low as 1.2 mg without binder. The SM and SOG-op can be processed from solutions in organic solvents. However, the most promising

result from Figure 31, is the dramatic increase of 48.75% in capacitance at current density of 10 mA g^{-1} as compared with the pure SM-based supercapacitors.

Next, to assess the capacitance retention over the CGCD at a constant current density of 0.1 A g^{-1}, it was performed for 10,000 cycles. As shown in Figure 32, the capacitance retention (C/C_0) can maintain over 86% after 10,000 CGCD, demonstrating a comparable stability to the supercapacitors from the polymeric nanocomposites with graphene-based materials. Furthermore, electrochemical impedance spectroscopy (EIS) was employed to assess the charge transfer resistance. As seen qualitatively in the Nyquist plots at different stages as an inset in Figure 32, after all the CVs, GCDs, and CGCD, the device reveals that the charge-transfer resistance at the final stage is lower than the initial, which is highly beneficial for superior electrochemical performance. It should be noted that graphene forms a conductive network and facilitates electronic and ionic transfer, minimizing the overall ionic resistance.

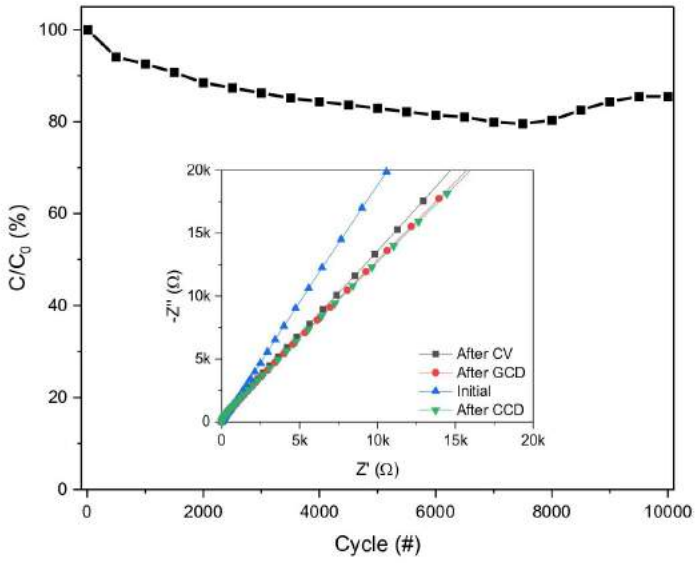

Figure 32 Capacitance retention over 10,000 Cycling Galvanostatic charge-discharge at 0.1 A g^{-1}. The inset shows an evolution of the Nyquist plot over the electrochemical sequence.

8. Conclusions

The main goal of the present work was to develop new materials and devices to provide solutions to the scientific and technological challenges related to energy storage. The synthesized 2D materials had size, crystallinity, dispersibility, and the number of layers controlled. A significant decrease in size above 90% from the starting 2D materials has been observed, without compromising other essential parameters, such as dispersibility, and the bandgap, which are very important to be used as an active layer.

A well-designed method allowed the synthesis of a novel graphene-based material that circumvents the trade-off between the properties of graphene and GO; the obtained SOG holds all the advantages of both materials without their drawbacks. The high crystallinity, low C/O ratio, high stability in water, and good conductivity, allowed the supercapacitors made with SOG to exceed the performance of the pure exfoliated graphene by ~17%, as seen in the CV and GCD curves where the high conductivity in conjunction with oxygen functionalities, enhance the faradaic capabilities to increase the pseudocapacitance contribution. In addition, the processability of SOG offers an easy implementation not only in supercapacitors but also opens the possibility of promising applications in printed organic electronics, energy storage devices, and organic solar cells.

The synthesized conjugated small molecule A-D-A was designed to have a low-lying energy level to accept electrons and interact well with the 2D materials by π-π stacking. To the best of our knowledge, this is the first work where a conjugated small molecule is used as an electrode of a supercapacitor device. It was shown that the capacitance value of 700 mF g^{-1} is relatively high when compared with polymer-based supercapacitors, even without the addition of binders. Furthermore, the most remarkable result is the outstanding increment by 48.75% in capacitance at 10 mA g^{-1} from the nanocomposite made of this SM and 10% SOG as compared to the one made from pure SM, demonstrating a synergistic effect in two-electrode Swagelok cells for a practical demonstration in energy storage. Additionally, after 10000 cycles, the capacitance retention was 85%. The results are encouraging and may open new research opportunities in this direction since this novel approach could potentially revolutionize the future design of electrode materials in supercapacitors. In particular, the Internet of Things (IoT) requires multifunctional materials that can work for both energy harvesting and storage, i.e., self-powering devices.

Acknowledgments

I gratefully acknowledge the financial support from the Knut and Alice Wallenberg Foundation (2017.0186) as well as funding from CONACYT under Grant Agreements *Becas nacionales* and *Becas de movilidad*.

I want to thank my supervisors. Chalmers, Prof. Ergang Wang, for being exceptionally supportive during all these years and for the excellent guidance and interesting research discussions. Cimav, Dr. Liliana Licea and Dr. Alfonso Pérez for giving me the opportunity to join and work in a highly collaborative research group and for their wonderful support and supervision.

Additionally, I would like to extend my sincere thanks to my examiners: Prof. Annette Larsson, Dr. Margarita Sánchez, Dr. Alfredo Morales, Dr. Pavel Vorobiev, Dr. David Meneses and Dr. Alejandra García for all their valuable feedback, suggestions and the time they took to review my work.

Heartfelt thanks to Krzysztof J. Kotewicz for allowing me to supervise his Master Thesis and his hard work. I'm delighted with your results and how they helped this thesis. Also, thank you for the nice discussions we always have about scientific matters and general gibberish, which always give me a different perspective, making you an excellent friend inside the lab and outside.

I would like to extend my sincere thanks to Wenhong, Petri, Cong, Jingnan, Qiaonan, Tadele, and Zewdneh for creating a unique work environment in the lab and giving excellent advice and suggestions. It is a pleasure to work with so nice people that shares all the energy and motivation. Special thanks to Qunping for teaching me polymers' synthesis and being a fantastic friend. Also, I'm deeply indebted to Birhan for being the best last minute (months) coauthor.

For all the administrative and technical help, many thanks to Lotta, Sara Da Costa, Anders Mårtensson, Nina Kann and Anne Wendel. I would also like to extend my thanks to my wonderful colleagues and the people I have shared the division of Applied Chemistry. Finally, I would like to thank to my old beloved friends from 8th floor Jessica, Amir, Xin. Special thanks to Jessica for all the help and coffee during the last stage of my PhD.

I would also extend my deepest gratitude to my parents, siblings, Alejandra, nieces, and nephews for always being super lovely and supporting me during all these years. No words are enough to thank you all.

Bibliography

1. R. E. Smalley, *Mrs Bulletin*, 2005, **30**, 412-417.
2. F. C. Krebs, *Polymer photovoltaics: a practical approach*, SPIE press Bellingham, WA, 2008.
3. R. F. Service, *Science*, 2005, **309**, 548-551.
4. N. Armaroli and V. Balzani, *Angewandte Chemie International Edition*, 2007, **46**, 52-66.
5. X. Huang, X. Qi, F. Boey and H. Zhang, *Chemical Society Reviews*, 2012, **41**, 666-686.
6. U. A. Méndez-Romero, M. Á. Velasco-Soto, L. Licea-Jiménez, J. Álvarez-Quintana and S. A. Pérez-García, in *Graphene Materials - Structure, Properties and Modifications*, ed. G. Z. K. a. A. C. Mitropoulos, IntechOpen, 2017, DOI: 10.5772/67474.
7. A. K. Geim and K. S. Novoselov, in *Nanoscience and technology: a collection of reviews from nature journals*, World Scientific, 2010, pp. 11-19.
8. K. S. Novoselov, A. K. Geim, S. V. Morozov, D. Jiang, M. I. Katsnelson, I. Grigorieva, S. Dubonos, Firsov and AA, *nature*, 2005, **438**, 197-200.
9. K. S. Novoselov, A. K. Geim, S. V. Morozov, D. Jiang, Y. Zhang, S. V. Dubonos, I. V. Grigorieva and A. A. Firsov, *Science*, 2004, **306**, 666-669.
10. R. Garg, S. Elmas, T. Nann and M. R. Andersson, *Advanced Energy Materials*, 2017, **7**, 1601393.
11. U. A. Méndez-Romero, S. A. Pérez-García, X. Xu, E. Wang and L. Licea-Jiménez, *Carbon*, 2019, **146**, 491-502.
12. C. H. A. Tsang, H. Huang, J. Xuan, H. Wang and D. Y. C. Leung, *Renewable and Sustainable Energy Reviews*, 2020, **120**, 109656.
13. S. Chen, X. Yu, M. Zhang, J. Cao, Y. Li, L. Ding and G. Shi, *Journal of Materials Chemistry A*, 2015, **3**, 18380-18383.
14. M. Bernardi, J. Lohrman, P. V. Kumar, A. Kirkeminde, N. Ferralis, J. C. Grossman and S. Ren, *ACS Nano*, 2012, **6**, 8896-8903.
15. Y.-J. Jeon, J.-M. Yun, D.-Y. Kim, S.-I. Na and S.-S. Kim, *Solar Energy Materials and Solar Cells*, 2012, **105**, 96-102.
16. S. Qu, M. Li, L. Xie, X. Huang, J. Yang, N. Wang and S. Yang, *ACS Nano*, 2013, **7**, 4070-4081.
17. I. Jung, D. A. Dikin, R. D. Piner and R. S. Ruoff, *Nano letters*, 2008, **8**, 4283-4287.
18. R. Garg, N. K. Dutta and N. R. Choudhury, *Nanomaterials*, 2014, **4**, 267-300.
19. M. A. Velasco-Soto, S. A. Pérez-García, J. Alvarez-Quintana, Y. Cao, L. Nyborg and L. Licea-Jiménez, *Carbon*, 2015, **93**, 967-973.
20. F. Zheng, W.-L. Xu, H.-D. Jin, X.-T. Hao and K. P. Ghiggino, *RSC advances*, 2015, **5**, 89515-89520.
21. J. M. Hollas, *Modern spectroscopy*, John Wiley & Sons, 2004.
22. E. V. Anslyn and D. A. Dougherty, *Modern physical organic chemistry*, University science books, 2006.
23. P. Murto, S. Elmas, U. A. Méndez-Romero, Y. Yin, Z. Genene, M. Mone, G. G. Andersson, M. R. Andersson and E. Wang, *Macromolecules*, 2020, **53**, 11106-11119.
24. H. Sun, X. Song, J. Xie, P. Sun, P. Gu, C. Liu, F. Chen, Q. Zhang, Z.-K. Chen and W. Huang, *ACS Applied Materials & Interfaces*, 2017, **9**, 29924-29931.
25. D. Meng, D. Sun, C. Zhong, T. Liu, B. Fan, L. Huo, Y. Li, W. Jiang, H. Choi, T. Kim, J. Y. Kim, Y. Sun, Z. Wang and A. J. Heeger, *Journal of the American Chemical Society*, 2016, **138**, 375-380.
26. R. Centore, L. Ricciotti, A. Carella, A. Roviello, M. Causà, M. Barra, F. Ciccullo and A. Cassinese, *Organic Electronics*, 2012, **13**, 2083-2093.
27. S. Chen, Z. Xue, N. Gao, X. Yang and L. Zang, *Sensors*, 2020, **20**, 917.
28. Y. Huang, W. Zhang, J. Wang and Z. Wei, *ACS Applied Materials & Interfaces*, 2014, **6**, 9307-9313.

29. F. Fernández-Lázaro, N. Zink-Lorre and Á. Sastre-Santos, *Journal of Materials Chemistry A*, 2016, **4**, 9336-9346.
30. H. Benten, D. Mori, H. Ohkita and S. Ito, *Journal of Materials Chemistry A*, 2016, **4**, 5340-5365.
31. E. B. Faulkner and R. J. Schwartz, *High performance pigments*, John Wiley & Sons, 2009.
32. J. C. Russell, V. A. Posey, J. Gray, R. May, D. A. Reed, H. Zhang, L. E. Marbella, M. L. Steigerwald, Y. Yang, X. Roy, C. Nuckolls and S. R. Peurifoy, *Nature Materials*, 2021, **20**, 1136-1141.
33. H. Wang, N. Jiang, Q. Zhang, G. Xie, N. Tang, L. Liu and Z. Xie, *Macromolecules*, 2021, **54**, 3469-3477.
34. A. De Adhikari, A. Morag, J. Seo, J.-M. Kim and R. Jelinek, *ChemSusChem*, 2020, **13**, 3230-3236.
35. S. Sharma, R. Soni, S. Kurungot and S. K. Asha, *The Journal of Physical Chemistry C*, 2019, **123**, 2084-2093.
36. A. V. Volkov, K. Wijeratne, E. Mitraka, U. Ail, D. Zhao, K. Tybrandt, J. W. Andreasen, M. Berggren, X. Crispin and I. V. Zozoulenko, *Advanced Functional Materials*, 2017, **27**, 1700329.
37. H. Li, J. Wang, Q. Chu, Z. Wang, F. Zhang and S. Wang, *Journal of Power Sources*, 2009, **190**, 578-586.
38. R. Wang, M. Han, Q. Zhao, Z. Ren, X. Guo, C. Xu, N. Hu and L. Lu, *Scientific Reports*, 2017, **7**, 44562.
39. A. Uddin and X. Yang, *J Nanosci Nanotechnol*, 2014, **14**, 1099-1119.
40. U. A. Méndez-Romero, S. A. Pérez-García, Q. Fan, E. Wang and L. Licea-Jiménez, *RSC Advances*, 2020, **10**, 29432-29440.
41. C. Vallés, F. Beckert, L. Burk, R. Mülhaupt, R. J. Young and I. A. Kinloch, *Journal of Polymer Science Part B: Polymer Physics*, 2016, **54**, 281-291.
42. D. Hou, Q. Liu, X. Wang, Y. Quan, Z. Qiao, L. Yu and S. Ding, *Journal of Materiomics*, 2018, **4**, 256-265.
43. D. A. C. Brownson, S. A. Varey, F. Hussain, S. J. Haigh and C. E. Banks, *Nanoscale*, 2014, **6**, 1607-1621.
44. M. Dresselhaus, A. Jorio and R. Saito, *Annu. Rev. Condens. Matter Phys.*, 2010, **1**, 89-108.
45. M. S. Dresselhaus, A. Jorio, M. Hofmann, G. Dresselhaus and R. Saito, *Nano letters*, 2010, **10**, 751-758.
46. A. C. Ferrari, *Solid state communications*, 2007, **143**, 47-57.
47. F. Boran and S. Ç. Gürer, *Turkish Journal of Chemistry*, 2019, **43**, 1322-1335.
48. Z. Wang, Q. Yao and S. Eigler, *Chemistry – A European Journal*, 2020, **26**, 6484-6489.
49. Q. Li, A. D. Smith, M. Haque, A. Vyas, V. Kuzmenko, P. Lundgren and P. Enoksson, *Journal of Physics: Conference Series*, 2017, **922**, 012014.
50. Q. Li, X. Guo, Y. Zhang, W. Zhang, C. Ge, L. Zhao, X. Wang, H. Zhang, J. Chen, Z. Wang and L. Sun, *Journal of Materials Science & Technology*, 2017, **33**, 793-799.
51. Y. Shao, M. F. El-Kady, J. Sun, Y. Li, Q. Zhang, M. Zhu, H. Wang, B. Dunn and R. B. Kaner, *Chemical reviews*, 2018, **118**, 9233-9280.
52. M. A. Bissett, I. A. Kinloch and R. A. Dryfe, *ACS applied materials & interfaces*, 2015, **7**, 17388-17398.
53. V. Skrypnychuk, N. Boulanger, A. Nordenström and A. Talyzin, *The Journal of Physical Chemistry Letters*, 2020, **11**, 3032-3038.
54. R. Kumar and M. Bag, *The Journal of Physical Chemistry C*, 2021, **125**, 16946-16954.
55. N. P. S. Chauhan, S. Jadoun, B. S. Rathore, M. Barani and P. Zarrintaj, *Journal of Energy Storage*, 2021, **43**, 103218.
56. Y. Zou, Z. Zhang, W. Zhong and W. Yang, *Journal of Materials Chemistry A*, 2018, **6**, 9245-9256.
57. N. Wang, X. Wang, Y. Zhang, W. Hou, Y. Chang, H. Song, Y. Zhao and G. Han, *Journal of Alloys and Compounds*, 2020, **835**, 155299.

58. M. Wang, H. Shi, P. Zhang, Z. Liao, M. Wang, H. Zhong, F. Schwotzer, A. S. Nia, E. Zschech, S. Zhou, S. Kaskel, R. Dong and X. Feng, *Advanced Functional Materials*, 2020, **30**, 2002664.
59. C. Wu, T. Zhou, Y. Du, S. Dou, H. Zhang, L. Jiang and Q. Cheng, *Nano Energy*, 2019, **58**, 517-527.
60. Y. Liao, H. Wang, M. Zhu and A. Thomas, *Advanced Materials*, 2018, **30**, 1705710.
61. N. An, Z. Shao, Z. Guo, J. Xin, Y. He, L. Lv, K. Xie, X. Dong, Y. Zhang and Z. Hu, *Journal of Power Sources*, 2020, **475**, 228692.
62. Y. Su, J. Du, D. Sun, C. Liu and H. Cheng, *Nano Research*, 2013, **6**, 842-852.
63. O. C. Compton and S. T. Nguyen, *small*, 2010, **6**, 711-723.
64. Y. Zhu, S. Murali, W. Cai, X. Li, J. W. Suk, J. R. Potts and R. S. Ruoff, *Advanced materials*, 2010, **22**, 3906-3924.
65. Y.-X. Wang, S.-L. Chou, H.-K. Liu and S.-X. Dou, *Carbon*, 2013, **57**, 202-208.
66. M. Forghani and S. W. Donne, *Journal of The Electrochemical Society*, 2018, **165**, A664-A673.
67. Y. Lin, H. Zhao, F. Yu and J. Yang, *Sustainability*, 2018, **10**, 3630.
68. J. Wang, J. Polleux, J. Lim and B. Dunn, *The Journal of Physical Chemistry C*, 2007, **111**, 14925-14931.
69. S. Fleischmann, J. B. Mitchell, R. Wang, C. Zhan, D.-e. Jiang, V. Presser and V. Augustyn, *Chemical Reviews*, 2020, **120**, 6738-6782.

CHALMERS UNIVERSITY OF TECHNOLOGY
Gothenburg, Sweden
www.chalmers.se

Tiny materials for huge energy storage

Two-dimensional (2D) materials, like graphene-based materials, are essentially single atomic layers of ordinary graphite used in the pencil's tip; they are so thin that they are not considered as 3D materials. As you might know, graphite, charcoal, and diamond are the same type of materials in terms of chemical element, but just different in atomic arrangement. 2D materials have very different and unique properties as compared to their counterparts, which grant them quite many interesting potential applications. On the other hand, conjugated small molecules (SM) are synthetic materials like the plastics around us but with fascinating electric properties like semiconductor. Conventional semiconductors like silicon are fragile, stiff, and expensive to produce and process. On the contrary, SM are solution-processable and can be easily produced and modified for target applications.

For a sustainable society, the supply of cheap and green energy is indispensable. Since renewable energy sources are often intermittent, it is crucial to store the produced energy. Supercapacitors are excellent candidates with numerous advantages: high-power density, ultra-fast charge-discharge, and long cycle life. However, the low energy density remains as its main drawback. In this thesis, through the proper modification of 2D materials and a conjugated small molecule, it was possible to increase by almost 50% energy density of the supercapacitors by a synergistic combination of these type of materials.

ULISES ANTONIO MÉNDEZ-ROMERO

2D materials and conjugated small molecules: from synthesis to devices for energy applications

2021

CHALMERS
UNIVERSITY OF TECHNOLOGY